Anisotropic Xe Chemical Shifts in Zeolites. The Role of Intra- and Intercrystallite Diffusion

Cynthia J. Jameson*

Department of Chemistry, University of Illinois at Chicago, 845 West Taylor, Chicago, Illinois 60607

A. Keith Jameson

Department of Chemistry, Loyola University, Chicago, Illinois 60626

Rex E. Gerald, II

Argonne National Laboratory, 9700 South Cass Avenue, Argonne, Illinois 60439

Hyung-Mi Lim

Department of Chemistry, University of Illinois at Chicago, 845 West Taylor, Chicago, Illinois 60607

Received: March 20, 1997; In Final Form: July 11, 1997[⊗]

We provide observations and interpretations of ^{129}Xe chemical shifts in open zeolite networks in which the Xe is in fast exchange among a large number of cavities and channels, in two zeolite types different from the A types that we have used before, and provide quantitative comparisons of adsorption isotherms and average ^{129}Xe chemical shifts using grand canonical Monte Carlo (GCMC) simulations employing the same methods and shielding functions used previously. We examine the temperature dependence of the Xe chemical shift at a fixed loading in NaY and silicalite and compare the predicted behavior with that of Xe_n in the α cages of NaA. Furthermore, we consider the most general case where the chemical shift reported by a Xe atom includes sampling environments in several crystallites and intercrystalline gas during acquisition of the NMR signal.

I. Introduction

The extremely high sensitivity of the ^{129}Xe NMR chemical shift to its environment has made the Xe atom a widely used probe in the characterization of microporous materials such as zeolites,[1−3] polymers, graphite, coals, and other materials. In zeolites the ^{129}Xe chemical shift is known empirically to depend on zeolite pore and channel dimensions,[4−8] on its Al/Si ratio,[9,10] cation distribution,[11] location of cations,[12] coadsorbed molecules, dispersed metal atoms, and paramagnetic ions, blockage of pores by coking, and domains of different composition or crystallinity. An understanding of the sensitivity of the chemical shift to these parameters is crucial to the quantitative application of the empirical observations. The relationship of the ^{129}Xe chemical shift to cavity size and shape, average Xe loading, temperature, and type of cations in zeolites is still not completely understood. If we can understand these relationships quantitatively, we should be able to make a clearer connection between the average chemical shift of the Xe signal under fast exchange with various parameters of the zeolite structure, although it may not be possible to predict a unique structure just from the average chemical shift.

The difficulties associated with establishing these relationships arise from the fact that the observed chemical shift in these open zeolite networks is the result of averaging over various environments. The established techniques of molecular dynamics and Monte Carlo computer simulations at the grand canonical level can provide details of distributions and dynamics of sorbate molecules. However, we had deferred using simulations to model the average chemical shift of the single Xe peak *under fast exchange* and its dependence on the temperature and loading until we have tested our methods with more detailed observations. To establish the connection between the observed chemical shift and specific attributes of the environment (such as cavity size and siting of cations), we have adopted the following strategy: (a) First make measurements in well-defined environments, propose a model for chemical shifts in these well-defined environments, and then test our ability to simulate the chemical shifts in these by using some statistical averaging method with our chemical shift model. We start with a sufficiently well-defined environment, a single zeolite cavity in which the locations of the atoms and ions are known independently, where the averaging of the chemical shift for a nucleus in a probe molecule trapped inside the cavity can be carried out using the chemical shift model, provided that a reliable description of the interaction between the probe molecule and the atoms and ions of the zeolite cavity is available. The averaging in this case is within one cavity. By experimentally changing the type and siting of the ions in this cavity while keeping the structure of the zeolite framework essentially unchanged, the chemical shift model and the description of the interaction can be tested against the experimentally observed chemical shifts. The chemical shifts in this case are for a fixed occupancy (*n* Xe atoms/cage is the occupancy associated with the ^{129}Xe chemical shift of Xe_n). Thus, chemical shifts in cages with identical occupancies and differing only in the type and siting of cations can be compared directly. Variable temperature measurements of the chemical shift averaged over a single cavity for a fixed occupancy (Xe_n) provide additional stringent tests. The average chemical shift in this case contains information about the one-body and two-body distributions of the probe molecules within a single cavity. How such a distribution is affected by type and siting of ions and by

[⊗] Abstract published in *Advance ACS Abstracts,* September 15, 1997.

S1089-5647(97)01013-4 CCC: $14.00

temperature are the types of information that can be checked, provided the chemical shift model is accurate. This first step establishes the connection between the distribution within a well defined environment such as a single cavity (given by GCMC simulations) and the observed chemical shift of a fixed known number of sorbate molecules. Effects of ion type, ion siting, and temperature can then be investigated experimentally and by simulations.

(b) The second step is to consider a large number of such cavities described in step a. Then we can discuss the distribution of the sorbate molecules among the array of cavities in a single crystallite. This distribution, if observed independently of the average chemical shift, is a test of the description of the interaction between sorbate molecule and a zeolite cavity convoluted with the description of the interaction between sorbate molecules. With experimental data of this kind we can then ask questions such as (1) For a given loading, what is the equilibrium distribution of sorbate molecules in a given microporous solid? (2) What factors influence the distribution? This itself is very relevant to technological applications of microporous solids in separations. Of equal importance is the partitioning of the sorbate molecules between the adsorbed phase and the bulk gas (the adsorption isotherm). The partitioning between bulk and adsorbed, as well as the distribution among cavities, are tests of the reliability of the descriptions of the intermolecular interactions. In the past, only the adsorption isotherm and the related quantity, the Henry's law constant, were used for this purpose. Only recently have measurements provided directly the distribution of molecules in zeolite cavities.[13,14]

(c) The third step in complexity is to allow the probe molecule to sample the environments in a large number of cavities of different occupancies, thereby averaging over the various occupation numbers, but still only providing an average of the inside environment of one crystallite, all of this occurring fast on the NMR time scale. This can be achieved by making measurements in a system with very large zeolite crystals. The observed average chemical shift contains information about the distribution of cavity occupation numbers in the crystallite, in addition to the distribution of the sorbate molecule within each cavity. The anisotropy of the internal environment and thus the anisotropy of the distribution of probe molecules within the crystallite will be reflected by the average chemical shift. Xe trapped in an environment of cubic or higher symmetry (tetrahedral, octahedral, icosahedral, or spherical) gives rise to an isotropic shift provided Xe is sufficiently mobile to undergo full intracage averaging. A review of examples in the literature of Xe occluded in nanoscale environments indicates that this is nearly always the case. For example, consider the isotropic lines observed in ^{129}Xe NMR spectra at occupancies of 6, 8, and 12 Xe/supercage in NaY at 77 K.[15] In this case, at 84° below the freezing point of bulk xenon, the interactions between the zeolite framework and Xe prevent the Xe atoms from achieving configurations appropriate to the symmetry of solid bulk xenon, thus the Xe inside the zeolite remains sufficiently mobile to exhibit complete intracage averaging. The supercages of NaY appear highly symmetrical to a Xe atom because the Na^+ ions are tucked away in sites outside the supercages. Other cages have varying degrees of anisotropy and *the average chemical shift reported by Xe in a single crystal, even at room temperature, depends on the orientation of the single crystal in the external magnetic field.*

(d) The fourth step is to consider the effects of exchange between several environments inside and outside the zeolite cavities and channels (intercrystallite diffusion) on the apparent ^{129}Xe chemical shifts and peak shapes. Since this is the most common type of measurement in applications using xenon to probe the structure of microporous materials, our goal is to interpret such experiments quantitatively and to understand the nature of the information being obtained under such conditions.

A. Averaging within a Single Cavity of Known Structure and Known Fixed Occupancy. Along this outlined strategy, we have accomplished the first and second steps. For this purpose we have used the model systems of Xe_n in NaA and KA cavities.[14,16] For the first step, the ^{129}Xe NMR spectra of the Xe atoms trapped in the α cages of zeolite NaA or KA give separate signals for each Xe_n, whose chemical shift represents an average within a single α cage of the zeolite. This model system clearly establishes the relation between the chemical shift and the occupation number of a cavity since the occupation number is known and unchanging during the course of the NMR interrogation for each Xe_n, even as the Xe loading is varied or the temperature changed. By directly comparing the chemical shifts of Xe_n in NaA with that in KA cavities, we have observed the effects of having K^+ ions instead of Na^+ ions on the ^{129}Xe NMR chemical shifts of Xe_n while the structure of the zeolite framework is essentially unchanged.[14,16] The temperature dependence of the chemical shifts at fixed known occupancy (i.e., for each Xe_n) has been studied in both NaA and KA cavities. We have verified these observations in grand canonical Monte Carlo simulations by reproducing the chemical shifts of Xe_n in NaA, as well as in KA, as a function of temperature, and in particular the differences between KA and NaA.[16,17] We have also examined the effects of the siting of K^+ ions on the ^{129}Xe chemical shifts of Xe_n.[16] Unlike simulations by others,[18−20] we have used the actual X-ray positions of framework atoms and extraframework ions in the simulation box, rather than idealized cages.

The chemical shift model we have used is one of pairwise additive intermolecular contributions. In other words, we assume that the chemical shift of Xe in a zeolite cage can be described by summing over the individual contributions from the Xe−O, Xe-cation, and Xe−Xe terms. From ab initio calculations of the argon cluster, Ar_3 and for Xe in CO_2, we have shown that, at distances appropriate to the configurations predominantly weighted in intermolecular interactions, the total isotropic shielding of the rare gas atom can be adequately described as a sum of atom−atom contributions to the intermolecular shielding.[21,22] In the gas phase, the density coefficients of the intermolecular chemical shift for Xe-rare-gas mixtures are themselves measures of this pairwise additive intermolecular chemical shift. By making the pairwise additive assumption for the Xe−zeolite chemical shift, it becomes possible to do a statistical averaging over all configurations of Xe within the zeolite cavity. (We have yet to address the conditions under which pairwise additivity breaks down.)

We carried out ab initio calculations of the effects of a zeolite framework on the NMR chemical shift of a rare gas atom using an ab initio analytical derivative theory[23,24] and gauge-including atomic orbitals (GIAO) for an Ar atom with selected neutral clusters which are 4-, 6-, or 8-ring fragments of the A zeolite cage. The locations of the Si, Al, and O atoms and the charge-balancing counterions (Na^+, K^+, and Ca^{2+}) of the clusters (from 24 to 52 atoms) are taken from the refined single-crystal X-ray structures and terminated with OH groups. In the spirit of our pairwise additive chemical shift model, the resulting shielding values of the Ar atom located at various positions relative to the cluster are fitted to a pairwise additive form to elicit effective individual Ar−O, Ar−Na, Ar−K, and Ar−Ca shielding functions of the form $\sigma(^{39}\text{Ar}, \text{Ar}\cdots\text{O}_{\text{zeol}}) = a_6 r^{-6} + a_8 r^{-8} + a_{10} r^{-10}$

$+ a_{12}r^{-12}$, where r is the distance between the Ar and the O atom. A similar form is used for the counterions. With these shielding functions a partitioning of the observed ^{129}Xe chemical shift of a single Xe atom in a cavity into cation and zeolite framework contributions was obtained.[25] The Xe-rare-gas shielding functions survived the test against the gas phase density coefficients previously measured in pure Xe gas and in rare gas mixtures over a range of temperatures.[21] The shielding functions for Xe−O and Xe-cation and Xe−Xe have survived the tests for the individual Xe_n chemical shifts in NaA and in KA.[16,17] That is, GCMC simulations of Xe in zeolites NaA and in KA using these shielding functions have reproduced the experimental chemical shifts and their temperature dependence for all Xe_n observations. These shielding functions have also been used in the GCMC simulations of Xe in the Ca^{2+}-ion-exchanged NaA, in which the chemical shifts of the individual Xe_n have been observed under magic angle spinning in $Ca_xNa_{12-2x}A$ cages ($x = 0, 1, 2, 3$).[26] None of the shielding functions used in these simulations were adjusted to agree with experiment. All of these experiments and the corresponding simulations are for Xe_n chemical shifts reporting only on the environments sampled within one cavity containing exactly n Xe atoms.

B. Equilibrium Distribution of Xe among an Array of Cavities in a Crystallite with No Exchange between Cavities. For the second step, we consider the distribution of sorbate molecules among the array of cavities within a zeolite in samples that have been determined to be in equilibrium with the bulk gas phase. Experimentally, we have directly observed in zeolite NaA individual ^{129}Xe NMR peaks for Xe, Xe_2, Xe_3, ..., Xe_8 whose intensities lead directly to the fractions $f(n)$ of the α cages containing n Xe atoms, i.e., the equilibrium distribution of Xe atoms among the cavities in the zeolite.[14] These distributions are dependent on Xe loading and temperature. The distribution of Xe in NaA has also been observed by others.[13,27,28] In addition, we have observed as a function of loading the distributions of Xe in KA,[16] and Ripmeester et al. have observed the distributions of Xe in AgA.[29] We have found that for a single component the distribution depends on the maximum occupancy of a pore (that is, it is related to the ratio of the pore volume to the sorbate volume), the overall average occupancy, and the interaction potentials between sorbate molecules.[14] We have reproduced the equilibrium distributions of Xe atoms among the cavities in 10 samples of Xe in NaA from low loading (0.45 Xe atoms/cage) to high loading (6.73 Xe atoms/cage) at 296 K and at 360 K by grand canonical Monte Carlo simulations.[17,30] We have also reproduced the equilibrium distributions of Xe atoms among the cavities in several samples of Xe in KA[16] and of Xe in AgA.[31] The rates of migration of Xe from one cage to another in these systems are slow enough for the observation of separate signals for cages with known occupancy numbers, and these rates of migration have been measured for Xe/NaA and Xe/AgA systems.[32−34]

The intermolecular potentials we have used for Xe−O and Xe-cation in these GCMC simulations have so far been adequate to reproduce the detailed distributions of cage occupancies as a function of loading in the Xe/NaA and the Xe/KA systems, and provided an adsorption isotherm for the Xe/NaA system that compared favorably with the room-temperature adsorption isotherm obtained by NMR at high loading.[17] We had not previously included polarization of Xe separately from the Lennard-Jones description of the Xe−zeolite interaction potential; we merely adjusted the Xe−O potential parameters to keep from getting cavity occupation numbers greater than 8 in NaA, to agree with experiment. This was done to avoid a multiplicity of adjustable parameters that would have been necessary if polarization were treated separately, and too many adjustable parameters would have clouded the straightforward interpretation of distributions and chemical shifts. Recently, we have treated polarization of Xe explicitly and now have a description of interactions of Xe with the zeolites NaA and KA which is equivalent to the all-Lennard-Jones Xe−O plus Xe-cation description in terms of its ability to reproduce the distributions and chemical shifts to almost within experimental error.[26] This description of interactions of Xe with A zeolites has tested successfully against the experimental chemical shifts of Xe_n in cavities of Ca-exchanged NaA, $Ca_xNa_{12-2x}A$, for $x = 0$, 1, 2, and 3. The explicit treatment of Xe polarization is essential to the interpretation of these experimental results. Furthermore, we obtain quantitatively the distributions of Xe among the cages of each type, $Ca_0Na_{12}A$, $Ca_1Na_{10}A$, Ca_2Na_8A, and Ca_3Na_6A, and we obtain semiquantitatively the partitioning of Xe in the competition among these types of cages in equilibrium with the same density of overhead Xe gas.[26]

C. Xe in Fast Exchange in Open Zeolite Networks. We carry out the third and fourth steps in this article. In this paper, we provide observations and interpretations of ^{129}Xe chemical shifts in open zeolite networks in which the Xe is in fast exchange, on the NMR time scale, among a large number of cavities and channels, in two zeolite types different from the A types that we have used before, and we provide quantitative comparisons using GCMC simulations employing the same methods and functions used previously.[17,26] For the third step we consider complete spatial sampling within a single crystallite. For a given crystallite the chemical shift average depends on the orientation of the crystallite with respect to the external magnetic field B_0. We provide a particularly convincing example of an anisotropic average of Xe chemical shifts in silicalite. An anisotropic average chemical shift arises from a weighted average of resonance frequencies resulting from (anisotropic) electronic nuclear shielding tensors associated with all Xe sites in a cavity environment which is spatially *anisotropic*. Thus, the observed chemical shift for Xe in a single cavity depends on the orientation of that cavity in the external magnetic field. Having survived the previous detailed tests in the first and second steps, our methods can now be used in this system (silicalite) which allows the probe molecule to sample the environments in a large number of cavities, thereby averaging over the various occupation numbers, but still only providing an average of the inside environment of one crystallite.

For the fourth step we investigate in the present work the effects of exchange between gas, intercrystalline, mesoporous, and occluded environments. That is, we are finally ready to attempt to interpret the most common type of measurement—that in which a single probe molecule reports not only on its sampling of the inside environment of a single crystal but of many crystallites as well as the gas in the intercrystalline region. At a given loading, the chemical shift average will depend on the temperature, since, as already established in the NaA and KA systems, the chemical shift average associated with each occupation number n and also the distribution of cavity occupation numbers within the crystallite vary with temperature, according to the description of the intermolecular interactions. At a given temperature, the chemical shift average will depend on the loading, since the distribution of cavity occupation numbers depends on the overall average occupancy. To use the measured ^{129}Xe chemical shift as a probe of environment, we need to know the totality of environments being averaged over. In this paper we consider the most general case, where the chemical shift reported by Xe atom includes sampling of

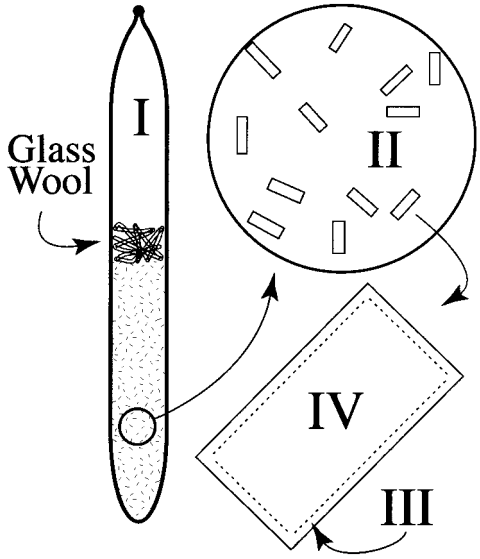

Figure 1. The various populations of Xe atoms in the sample that contribute to the observed ^{129}Xe NMR spectrum are in reservoir I, the overhead Xe gas, reservoir II, the intercrystallite Xe, some of which may be adsorbed on the outside surface of the zeolite, reservoir III, intracrystallite Xe within diffusive distance of the outside, and reservoir IV, intracrystallite Xe deep inside the crystallites, incapable of exchanging with the outside Xe within the NMR time scale.

environments in several crystallites and in the gas in the intercrystalline region. In doing this, we call attention to the necessity of understanding the dynamics in order to make proper use of the sorbate chemical shift as a probe of environment. To make the connection between the ^{129}Xe chemical shift in a sample and the zeolite structure in this most general type of measurement, it is important to know the various populations of Xe atoms that contribute to the observed peak. We may consider Xe populations distributed in the sample space as follows: *Reservoir I* includes the Xe atoms that are in the overhead gas, far away from the crystallites and incapable of exchanging with the "inside" Xe within the NMR time scale. *Reservoir IV* includes the Xe deep inside the crystallites that are incapable of exchanging with the Xe atoms outside within the time required to record an NMR spectrum. *Reservoir III* includes the Xe atoms inside the crystallites that are within an exchangeable layer near the outside. *Reservoir II* includes the Xe atoms found between the crystallites, some of which may be adsorbed on the outside surface of the zeolite, and capable of exchanging with the Xe atoms in reservoir III. These reservoirs are shown schematically in Figure 1. The relative volumes of these reservoirs depend on morphology and size of crystallites, crystallite packing, and overhead Xe gas pressure. In the limit of very large crystals there are effectively only reservoirs I and IV. In the limiting case of very fine powder filling up that part of the sample tube within the receiver coil in the NMR experiment, there are effectively only reservoirs II and III. We offer observations and interpretations in both of these limiting cases in this paper.

II. Experimental Section

A. Sample Preparation. The typical sample tube is made from ordinary borosilicate glass tubing of nominal 4 mm o.d. and about 5 cm in length from the test tube bottom to a slightly necked-down portion. For safety reasons it is essential to anneal the tubes in a commercial annealing oven at this juncture to remove stresses. The tube volume is calibrated with mercury, then previously dried zeolite is added, a small glass wool plug is inserted (see Figure 1) to keep the zeolite in place, and the tube carefully flame-narrowed above the center of the necked-down region to provide for a minimal area of stress in the final sample tube. The resulting assembly is then dried at 350 °C under vacuum for at least 16 h under "thin-bed" conditions (a bed thickness of about 1−1.5 mm) to remove residual water which may have been introduced in handling the zeolite. Use of a Young-type stopcock allows easy transfer from the drying vacuum line to a standard line in which a measured amount of xenon can be introduced, without loss of vacuum at any previous time. The final sample is flame-sealed under liquid nitrogen, has an accurately known (±2%) volume of about 0.2 mL, contains a known mass of zeolite (about 25 mg), and a known number of moles of xenon. Our experience indicates that these samples will routinely withstand internal pressures of at least 50 atm.

We also prepared samples of Xe in zeolite NaX. The NaX crystallites were ca. 1 μm, obtained from Linde (13X). Our samples of NaX zeolite have a deduced formula of $Na_{88}Al_{88}Si_{104}O_{384}$, that is, a Si/Al ratio of 1.18. The Si/Al ratio was calculated from the relative intensities of the individual Si nuclear sites distinguishable by means of their ^{29}Si chemical shift in the ^{29}Si MAS NMR spectrum, as demonstrated by Engelhardt et al.[35]

The sample of pure silicalite was generously donated by Judith Melville of AMOCO. This sample of silicalite was 100% crystalline, $V_{\text{unit cell}} = 5345$ Å^3, cation-free, <24 ppm Al, and 42.4% Si. The submicron size crystallites are clumped together, forming aggregates of micron size. This zeolite was dried overnight at 350 °C under thin-bed conditions (<2 mm).

Large crystals of silicalite were synthesized using chemicals from Aldrich (98+% purity) according to ref 36. A typical sample preparation included mixing, under nitrogen atmosphere, 0.527 mL of deionized H_2O, 0.8 mL of propylamine, 8.0 mL of triethylamine, and 0.5 mL of triethylamine trihydrofluoride in a 23 mL Parr Teflon-lined general purpose bomb (model 4745, Parr Instrument Co., Moline, IL). To that solution was added 0.573 g of fumed silica (SiO_2) and 0.649 g of tetrapropylammonium bromide, mixed in a separate weighing container. The resulting thick slurry was stirred to a uniform wetted mix. The sealed reaction vessel was placed in a dedicated oven heated to 450 K. The oven temperature was monitored daily and remained constant to within one degree over the course of the reaction. The reaction vessel was removed after 14 days and allowed to cool. A successful synthesis resulted in 99+% yield of large ($200 \times 100 \times 20$ μm^3) single crystals of silicalite with uniform size and morphology (see Figure 2). Samples made from the large crystallites were treated in the same way and sealed with xenon in glass tubes as described above. In addition, a special sample of these crystals was prepared in a capillary tube, (nominally 0.9 mm i.d. and 1.5 mm o.d.) in an attempt to preferentially align them along the axis of the capillary tube. Individual single crystals were loaded into the capillary tube using fine tweezers under a stereomicroscope. The capillary tube was connected to a vacuum line and heated to 573 K overnight, then xenon gas (99.95% ^{129}Xe) was condensed in the tube using liquid nitrogen. The flame sealed tube measured 28 mm in overall length.

B. NMR Spectroscopy. The spectra of this capillary tube sample were taken using a microprobe. A microcoil NMR probe (ref 37) was fabricated by winding 30 turns of 42 gauge enamel-coated copper wire directly onto the sample capillary tube. The tube was suspended at both ends by two Vespel posts which were mounted to a Torlon base. The coil was glued to the capillary tube with Superglue and tuned to 110.639 MHz using ceramic capacitors of fixed values. The capillary tube

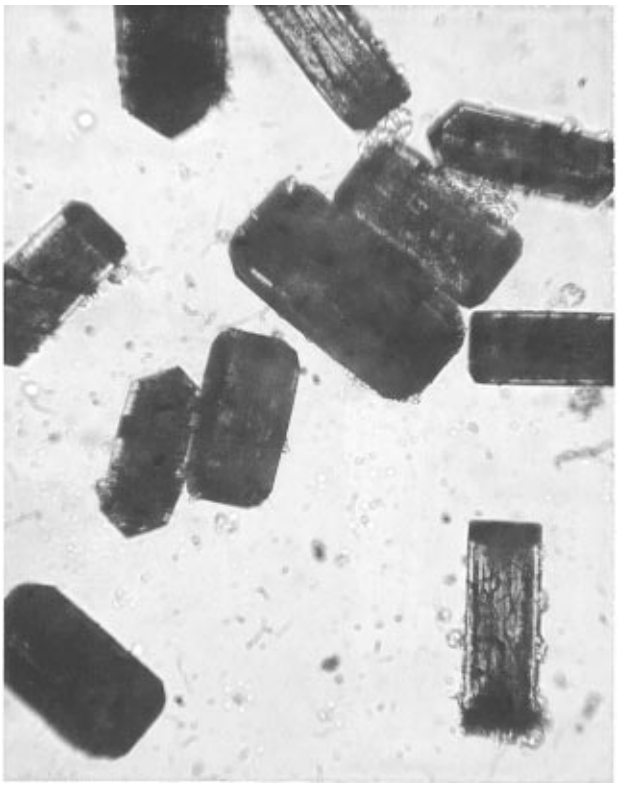

Figure 2. Single crystals of silicalite synthesized as described in the text. The large crystal in the center of the photograph measures 288 × 144 × 20 μm.

was submerged into a small polycarbonate cup containing poly(dimethylsiloxane) as a susceptibility matching fluid. In this manner, external magnetic field gradients across the 0.9 mm sample tube diameter were reduced by a factor of 2; similar results could not be achieved with the spectrometer's room-temperature shims. Because of the large crystals and their random orientation in the capillary tube, it is reasonable to expect inhomogeneous line broadening due to anisotropic diamagnetic susceptibility. A pulse duration of 1 μs was sufficient to uniformly saturate all the xenon magnetization in the capillary sample using the standard rf amplifiers on a Varian UNITY 400 spectrometer.

The ^{129}Xe NMR spectra from Xe introduced into these large crystals in the regular 4 mm sample tube were taken on a Bruker AC200 spectrometer (employing a Nalorac 5 mm broadband probe). The spectra are shown in Figure 3 for both the regular sample with 43 mg of silicalite (41 000 scans) and the capillary sample with 7 mg (1024 scans). The spectrum in the capillary sample may appear to be better defined but the packing may not be completely random. This is the first report of a ^{129}Xe NMR spectrum for occluded Xe in a zeolite exhibiting a definite powder pattern at room temperature, although Ripmeester and Ratcliffe have reported powder patterns at room temperature for Xe in an aluminophosphate.[38] From spectrum a in Figure 3 taken in the regular sample tube we obtain $\delta_{11} = 187.9$ ppm, $\delta_{22} = 179.4$ ppm, and $\delta_{33} = 163.5$ ppm, the average value being 176.9 ppm.

To obtain $\langle N \rangle_{Xe}$ by Xe mass balance, we use the known volume of the sample, the known total number of Xe atoms introduced, and the known number of unit cells from the mass of zeolite introduced. We deduce the number of Xe atoms in the zeolite from the density of Xe gas in equilibrium with the adsorbed xenon. We obtain the density of Xe in the gas in equilibrium with the sample from a chemical shift measurement, since we know the density and temperature dependence of the

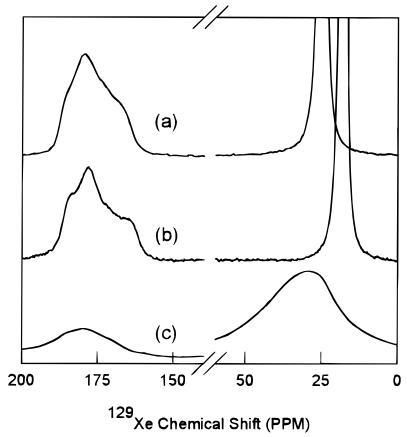

Figure 3. ^{129}Xe NMR spectrum of Xe in large crystals of silicalite at 300 K at loadings $\langle N \rangle_{Xe} = 16$ Xe atoms/unit cell, (spectrum a) in a standard sample tube, as described in the text, employing a standard 5 mm probe, (spectrum b) in a capillary sample tube employing a microprobe, as described in the text, are compared with the Xe spectrum in (spectrum c), microcrystalline silicalite at the same temperature and loading.

Xe chemical shift in pure Xe gas from previous work.[39] It is important to measure the actual Xe chemical shift in the gas, rather than some average weighted by exchange with the Xe atoms inside the zeolite. In these samples the density of the gas in equilibrium with the adsorbed Xe is taken experimentally from the resonance frequency of the gas in the inverted sample, such that only reservoir I is in the receiver coil. For the overhead gas spectra, a pulse width of $\pi/6$ was used with a recycle time of about 60 s. The chemical shift of the gas-only signal is converted into a value for the gas density. (Our sample is fully dewared in both configurations because of its small size.) In turn, the density provides the number of Xe atoms in the gas phase and by difference, the number of Xe atoms in the adsorbed phase. If we assume that, at room temperature, the fraction of the total Xe in the sample that is adsorbed on the surface of the crystallites (reservoir II) is small compared to the fraction that is occluded inside (reservoir IV), we can get $\langle N \rangle$, the number of Xe atoms per unit cell. The assumption that at room temperature the fraction adsorbed on the surface of the crystallites (reservoir II) is negligible is not always valid. Fortunately, we also have the chemical shift to indicate whether the number of Xe atoms inside the zeolite has reached the maximum occupancy.

C. Magnetization Transfer and Hole-Burning Experiments. We attempted magnetization transfer experiments on samples of xenon in microcrystalline silicalite. These experiments failed because the time required to selectively spin label the nuclei of either the occluded or the interparticle xenon atoms was long compared to the reciprocal of the exchange rate. Therefore, a selective inversion of either magnetization resulted in a substantial saturation of the other. However, it is possible to selectively invert either the occluded or the interparticle xenon magnetization in the samples with large crystals of silicalite. Experimentally measured rates for xenon magnetization exchange between the inside of the porous particles (reservoir IV) and the outside interparticle (gas) phase (reservoir II) contains intrinsic information about transport parameters of xenon atoms in the interior of the particle, at the gas−surface interface, and in the gas phase. The steady-state ^{129}Xe NMR spectra of these systems are determined by chemical shifts at all intraparticle and interface sites as well as in the interparticle gas phase, weighted according to the intrinsic rate constants for intraparticle site exchange (which combine to give intraparticle

diffusion), exchange at the gas−solid interface, and gas-phase diffusion weighted by the xenon populations. The dynamic ^{129}Xe NMR spectra of these systems are determined by the weighted transport properties taken together with rate constants for energy exchange between xenon nuclei and the different environments. Xenon magnetization transfer experiments therefore afford a plethora of information which in many systems is difficult to distill into the intrinsic components because several sample parameters are ill-defined (e.g., particle morphology, size distribution, and sample packing). For a system of xenon atoms and large crystals of silicalite, it may be possible to extract the self-diffusion coefficient for xenon in silicalite by the analysis of xenon magnetization transfer experiments. This is made possible because the larger crystals of silicalite have a very small surface-to-volume ratio, are of well-defined size with a narrow particle size distribution, and have a single morphology.

Magnetization transfer experiments were conducted by selectively inverting the magnetization for occluded xenon (the powder pattern) and the interparticle xenon (the gas peak), each in turn using the selective echo chemical shift imaging (SECSI) pulse sequence.[40] For xenon/zeolite systems whose ^{129}Xe NMR spectrum is composed of two chemical shifts, the SECSI pulse sequence provides the shortest preparation period for selectively inverting the magnetization of either xenon reservoir. Whereas the modified DANTE pulse sequence we used in ref 32 required approximately 0.5 ms to effect selective magnetization inversion, preparation periods employing the SECSI method were as short as 0.044 ms with the microcoil probe. The SECSI sequence consists of three $\pi/2$ pulses each of duration 7.5 μs separated by two delays. The first delay is the antiphase period which for the Xe/silicalite system was 0.029 ms. The second delay is the mixing period during which the xenon atoms in the spin labeled reservoir exchange with xenon atoms from the other reservoir. The third radiofrequency pulse transfers the encoded z magnetization to $x-y$ magnetization for detection. The 26 or 32 mixing periods used for the magnetization transfer experiments reported here range from 0.025 to 15 s. Each spectrum resulted from signal averaging 128 (or 256) transients with a recycle delay of 15 s. A spectral width of 40 kHz was acquired using 4096 points. The free induction decays were processed with a line broadening of 100 Hz.

Hole burning experiments were carried out in silicalite. A modified DANTE sequence consisted of a series of 16 $\pi/16$ pulses to produce the selective π pulse, with a cyclical 90° phase shift between each pulse pair. In this manner the selective frequency is not at the central spectrometer frequency, but at offset frequencies $(4n + 1)\nu$ where $n = 0, \pm1, \pm2, ...$, and ν can either be positive or negative depending on the sense of the phase cycling. Each of the 16 pulses is of duration 1.0 μs. The separation of DANTE pulses is 0.15 ms. This achieved a selective peak inversion at +1800 Hz and −3(1800) Hz in the 20 kHz sweep width used.

III. Results

A. Xe in Silicalite. ^{129}Xe NMR spectra of Xe in the small crystallites of silicalite (shown in Figure 4) provide a good example of dynamics affecting the apparent Xe chemical shift, especially in the high-loading samples. The 13 samples of Xe in microcrystalline silicalite including loadings ranging from 1.75 Xe atoms/unit cell up to saturation. Spectra of the overhead gas, shown as insets in Figure 4, taken with the sample tubes inverted so that none of the packed zeolite is in the receiver coil, can routinely be observed for loadings above 10 Xe atoms per unit cell. (For very low Xe gas densities one could nearly always measure a gas signal provided one takes into account that the relaxation times are much longer.) The gas peak observed in this way is very sharp in these cases (ca. 0.01 ppm wide), as opposed to the much broader peaks shown in the full spectrum of the packed microcrystalline powder, where no hint of a separate, sharp gas peak can be seen. (See Figure 4.) The values of $\langle N\rangle_{Xe}$ shown in Figure 4 are apparent values obtained by mass balance, by using the chemical shift of ^{129}Xe in the overhead gas to determine the density of the gas, and do not reflect the actual occupancies within a unit cell. In aggregates of clustered microcrystals, the intercrystalline void space have dimensions comparable to the intracrystalline channels, thus the apparent $\langle N\rangle_{Xe}$ values reflect the total adsorbed phase, including the xenon adsorbed in the mesopores formed by the microcrystal aggregates. At low loading, the $\langle N\rangle$ shown in Figure 4, obtained by assuming that all the xenon is adsorbed (no overhead gas peak), is reasonably accurate.

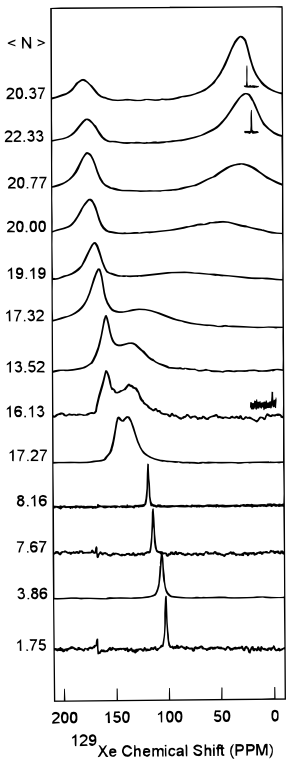

Figure 4. ^{129}Xe NMR spectra at 300 K of Xe in microcrystalline silicalite at various loadings from around 1 Xe atom per unit cell, up to saturation. For selected samples the observed overhead gas spectrum is also shown as an inset (see text). The calculated values of $\langle N\rangle_{Xe}$ (number of Xe atoms per unit cell), based on the density of the overhead gas, are indicated to the left of the figure.

We now compare the ^{129}Xe NMR spectra in the microcrystalline samples with that in the large crystals of silicalite. In Figure 3 we compare samples at nearly equal loadings, the overhead gas peaks indicating about 48−50 amagat of Xe. The microcrystalline sample spectrum c shows two very broad featureless peaks, the "gas" peak being noticeably shifted to higher chemical shift in comparison to the overhead gas. On the other hand, the gas peak in the sample of xenon in large crystals of silicalite shown in spectrum a has the same chemical shift as the overhead gas observed in the inverted tube. Spectrum c is indicative of a large fraction of the Xe population being involved in exchange between the adsorbed phase and the gas phase, whereas a much smaller fraction of the Xe population is involved in exchange in spectrum a. The magnetization transfer experiments in sample a give a measure of this exchange rate. (See magnetization transfer results below.)

With so much Xe adsorbed in the intercrystalline mesopore reservoirs (reservoir II) of microcrystalline silicalite samples, it is not possible to determine the true $\langle N \rangle_{Xe}$ in the sample by mass balance. At higher overhead gas densities, the number of Xe atoms adsorbed on the outside surfaces of the silicalite microcrystallites can be significant, up to as much as 6 Xe atoms/unit cell beyond the full occupancy of the large crystals of silicalite. In the microcrystalline samples of silicalite, full occupancy is reached when the *apparent* loading is 20 Xe atoms/unit cell at room temperature. This agrees with Cheung's report that the observed maximum capacity of silicalite was 3.5 mmol of Xe/g or 20 Xe atoms/unit cell at 144 K.[41] Cheung's samples were very likely of similar morphology, very fine crystals clumped together, with mesopores between microcrystallites. At 144 K, they found that any excess Xe merely formed solid bulk Xe on the outside of the silicalite and that it could be clearly distinguished by its chemical shift, 304 ppm at 144 K. However, the Xe in the mesopores would not freeze at the same temperature as bulk xenon on the outside of the aggregates, and it would appear to be inside the channels of individual crystals.

When the crystals are very large, the fraction of Xe atoms that are within diffusive distance of the outside surface (i.e., in reservoir III) is small, so the true chemical-shift average of the occluded (reservoir IV) Xe atoms is observed, as in the spectra in Figure 3, rather than a somewhat smaller apparent chemical shift partially averaged with the gas phase that is observed in the spectra in Figure 4. The fraction of Xe atoms which are adsorbed on the outside surface of large crystals is much smaller too, so that the intercrystalline (reservoir II) Xe signal is very sharp and appears at the same chemical shift as the overhead gas (reservoir I). In Figure 3 we compare a ^{129}Xe NMR spectrum for occluded Xe in the large crystals of silicalite (spectrum a) with that obtained in the microcrystalline samples (spectrum c). In the large crystals, the reservoir IV Xe atoms exhibit a powder pattern, which is not washed out by averaging between crystallites at various orientations. The same limiting value of the isotropic chemical shift for reservoir IV is reached in the large crystals as in the microcrystallites. At high overhead pressures of Xe gas at room temperature, we find that the limiting chemical shift of Xe in reservoir IV is reached when the loading is 16 Xe atoms/unit cell in the large crystals of silicalite. It has been suggested that the maximum occupancy is 16 Xe atoms/unit cell,[42,43] rather than the 20 Xe atoms/unit cell, reported by Cheung,[41] or the comparable number that results from some molecular dynamics simulations.[44] Experimental measurements at 195 K gives an adsorption isotherm that is type I with a maximum adsorption of 16 Xe atoms/unit cell of silicalite.[45] This is the same as what we find as the maximum capacity. In a grand canonical Monte Carlo simulation of Xe in silicalite, the Kiselev potential gives a type I isotherm at 195 K with a maximum adsorption of 18 Xe atoms/unit cell, while the Pellenq−Nicholson potential gives a maximum adsorption of 16 molecules/unit cell.[42] In molecular dynamics simulations using 16 Xe atoms/unit cell at 400 K, the channels are far from completely packed,[46] and maximum capacity has been estimated at about 20 Xe atoms/unit cell,[44] while other molecular dynamics simulations suggest that 16 Xe atoms/unit cell is close to the maximum packing.[43] The disagreement in the estimates of maximum Xe occupancy ranging from 16 to 20 Xe atoms/unit cell is an indication of the differences between the various potential parameters used in the simulations.

In the microcrystalline silicalite samples, the apparent Xe chemical shift increases rather significantly with increasing $\langle N \rangle_{\text{adsorbed Xe}}$ and then levels off at an average chemical shift for Xe of 180 ppm. The ^{129}Xe chemical shift in the adsorbed phase is plotted against the calculated $\langle N \rangle_{\text{adsorbed Xe}}$ in Figure 5, where we show the true chemical shifts corresponding to Xe in reservoir IV (n) and the apparent chemical shifts obtained from the microcrystalline samples. The apparent $\langle N \rangle_{\text{adsorbed Xe}}$ in Figure 5 from mass balance is not the correct $\langle N \rangle_{Xe}$ for reservoir IV in the microcrystalline silicalite, due to substantial intercrystalline adsorption already discussed above. The scatter in $\langle N \rangle_{\text{adsorbed Xe}}$ is consistent with a relative standard deviation in the loading of about 10%. This arises because of the mass balance procedure requiring the subtraction of a substantial fraction of the xenon in the sample, which is in the gas, to deduce the number of moles in the solid phase. Propagation of errors from an expected error in the volume of the sample tube available to the gas (about 2%) accounts for a major part of the scatter. In addition, the degree of packing of microcrystalline material is not uniform from one sample to the next.

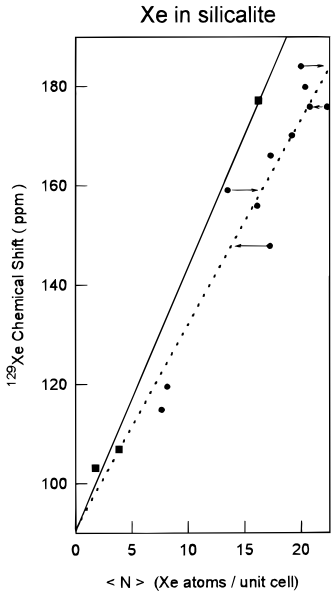

Figure 5. The dependence of the ^{129}Xe chemical shift (relative to the isolated Xe atom) upon $\langle N \rangle_{Xe}$ for Xe in silicalite at 294 K in the microcrystalline silicalite (●) and in the large crystals (■), taken from the spectra in Figure 4 and in large crystals. The scatter in $\langle N \rangle_{Xe}$ is consistent with a relative standard deviation in the loading of about 10% (see text).

In the very low-loading samples, the exchange is very fast and the chemical shift is an average of the inside Xe and the gaseous Xe. However, there is essentially no gas, so the observed chemical shift corresponds to that of Xe inside the unit cells of the silicalite. At medium loading the apparent chemical shift of the adsorbed phase in the microcrystalline samples is a result of averaging with the gas due to exchange at substantial gas densities. When the crystallites are small, there is a sizable fraction of Xe atoms in reservoir III; the apparent chemical shift in the adsorbed phase is too low, reflecting an environment partially averaged with the Xe atoms in reservoir II. Thus, they do not agree with the (true) chemical shifts of xenon adsorbed within the large crystals, as seen in Figure 5. The apparent chemical shift of the gas signal from the Xe atoms in reservoir II is also too high because of this partial averaging.

We note the temperature dependence of the powder pattern in silicalite in Figure 6, where both the spectra at 300 K and at 240 K correspond to maximum loading. We believe the loading to be maximum in that sample at 300 K, thus, as temperature decreases, the loading stays at maximum for each temperature, increasing slightly with decreasing temperature. The gas peak

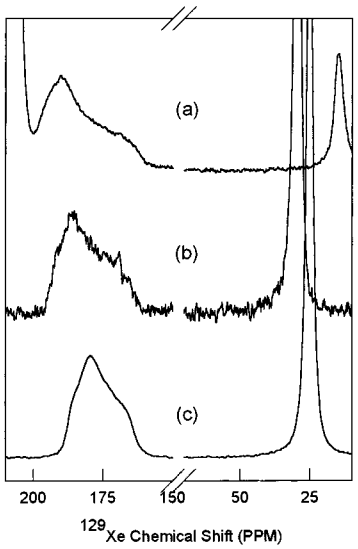

Figure 6. Comparison of ^{129}Xe NMR spectra at maximum loading of Xe in large crystals of silicalite at 240, 270, and 300 K. The characteristics of the powder patterns correspond to (spectrum a) 240 K, $\delta_{11} = 199.3$, $\delta_{22} = 189.4$, and $\delta_{33} = 161.9$ ppm; (b) 270 K, $\delta_{11} = 193.4$, $\delta_{22} = 185.6$, and $\delta_{33} = 163.5$ ppm; (spectrum c) 300 K, $\delta_{11} = 187.9$, $\delta_{22} = 179.4$, and $\delta_{33} = 163.5$ ppm. At 240 K an intense bulk liquid xenon peak at higher chemical shift, which forms on the exterior of the crystals, is observed. The number of scans taken for these spectra are respectively 10 600, 1500, and 29 000 for spectra a, b, and c.

shifts to greater chemical shift in going from 300 K (Figure 6, spectrum c) to 270 K (Figure 6, spectrum b) according to ref 39,

$$\sigma(T,\rho) = \sigma_0 + \sigma_1(T)\rho + \sigma_2(T)\rho^2 + ...$$

the chemical shift being $\delta = -[\sigma(T,\rho) - \sigma_0]$, relative to the free Xe atom. At constant density the chemical shift of the gas moves to greater values with decreasing temperature, according to the known temperature dependence of the virial coefficients of shielding in this equation. At 240 K an intense bulk liquid Xe peak is observed which appears at higher chemical shift than the powder pattern (Figure 6, spectrum a). The bulk liquid forms on the exterior of the crystals. The remaining gas is at a much lower density ($\delta_{Xe} = 14.8$ ppm, appropriate to a density of 22 amagat), in equilibrium with the liquid at 240 K.

We observe a change in the powder pattern in the large crystals of silicalite with decreasing temperature in Figure 6. The anisotropy in the average tensor becomes more pronounced at lower temperatures. The values of δ_{11} and δ_{22} appear to be noticeably temperature dependent, while δ_{33} appears to be almost temperature independent. δ_{11} and δ_{22} represent averages of chemical shift tensor elements, each of which has a large dispersion (range of values). δ_{33} also represents an average for a range of tensor-element values, but with a smaller dispersion. The larger magnitude of the dispersion for δ_{11} and δ_{22} compared to that for δ_{33} (obtained from their temperature dependence, seen in Figure 6) provides additional information.

Magnetization transfer experiments were carried out to determine the rate of the exchange between the adsorbed and gas phase Xe. The results are shown in Figure 7. The peaks from a similar series of spectra with a greater signal to noise ratio were integrated and plotted in Figure 8. Since the signal for reservoir II remains unperturbed during a selective inversion of the signal from reservoir IV (powder pattern) a condition easily achieved here due to the 200 ppm separation of the signals for reservoirs II and IV, then $M_{II}^0 = M_{II}^\infty$,and $M_{IV}^0 = -M_{IV}^\infty$.

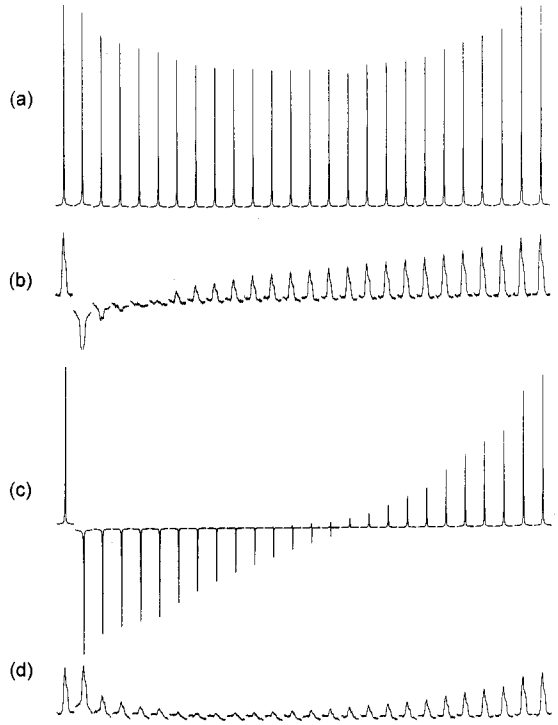

Figure 7. Magnetization transfer experiments for Xe in large crystals of silicalite. Delay times are 15, 0, 0.025, 0.05, 0.075, 0.1, 0.2, 0.3, 0.4, 0.5, 0.6, 0.7, 0.8, 0.9, 1, 1.2, 1.4, 1.6, 1.8, 2, 2.5, 3, 3.5, 4, 7, and 10 s. Spectra a and b: the magnetization as a function of delay time upon selective inversion of the powder pattern from reservoir IV. Spectra c and d: the magnetization as a function of delay time upon selective inversion of the gas (reservoir I/II) peak.

For this case, the equations to be fitted to the recovery curves in Figure 8 are

$$M_{IV}(t) = M_{IV}^\infty + [(M_{IV}^\infty - M_{IV}^0)/(\lambda_1 - \lambda_2)]\{(\lambda_2 + k_{1,IV})e^{\lambda 1 t} - (\lambda_1 + k_{1,IV})e^{\lambda 2 t}\}$$

$$M_{II}(t) = M_{II}^\infty - [(M_{IV}^\infty - M_{IV}^0)/(\lambda_1 - \lambda_2)]k_{IV}\{e^{\lambda 1 t} - e^{\lambda 2 t}\}$$

where

$$\lambda_1 = {}^1/_2\{-(k_{1,IV} + k_{1,II}) + [(k_{1,IV} - k_{1,II})^2 + 4k_{IV}k_{II}]^{1/2}\}$$

$$\lambda_2 = {}^1/_2\{-(k_{1,IV} + k_{1,II}) - [(k_{1,IV} - k_{1,II})^2 + 4k_{IV}k_{II}]^{1/2}\}$$

and $k_{1,IV} = k_{IV} + 1/T_{1,IV}$ and $k_{1,II} = k_{II} + 1/T_{1,II}$. Signal intensities (integrated areas) are used rather than peak heights in the analysis. From the fitting we obtain k_{IV}, the rate constant for leaving the adsorbed phase (reservoir IV) to go into the gas phase (reservoir II) and k_{II} for leaving the gas to enter the adsorbed phase. By assuming this 2-site exchange mechanism, we forced a fit to the data.[47,48]

$$k_{IV} = 3.0\ s^{-1}$$

$$k_{II} = 1.39\ s^{-1}$$

These are only approximate values because we have found (see Figure 8) that a simple two-site exchange mechanism does not provide as good a fit as the precision of the experimental data. We consider the dynamics in this system in more detail in a later paper.[49]

Additional evidence that the powder pattern corresponds to inhomogeneous broadening is provided by hole-burning experi-

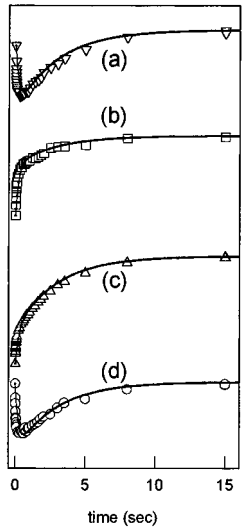

Figure 8. Magnetization transfer experiments for Xe in large crystals of silicalite. Spectra a and b are the responses of the gas (reservoir II) and occluded (reservoir IV) peaks, respectively, after selective inversion of the occluded peak (magnetization as a function of delay times upon selective inversion of the powder pattern). Spectra c and d are the responses of the gas and occluded peak after selective inversion of the gas peak. (The magnetization as a function of delay times upon selective inversion of the gas peak). The curves are the fit using the rate constants given in the text.

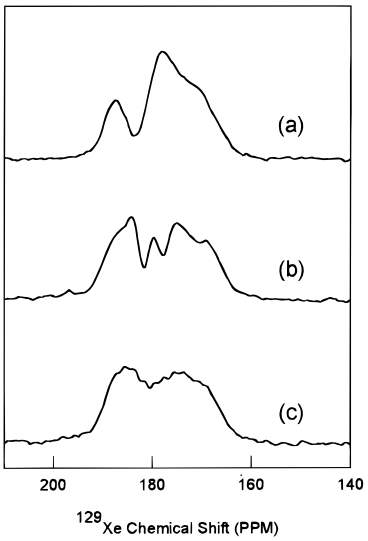

Figure 9. Hole-burning experiment in the powder pattern of Xe inside large crystals of silicalite. Delay times are spectra a, 0.3 μs; spectra b, 0.03 s; spectra c, 0.20 s.

ments where we saturated a narrow region of the powder pattern but left the remainder essentially unaffected. Figure 9 shows a hole approximately 300 Hz wide burned in the powder pattern. Because the pulse sequence used lasted for a time less than T_1, the hole represents a highly selective inversion of a subset of crystal orientations in the sample. The effect of the strong irradiation is essentially confined to the signal coming from only those Xe atoms in large crystals having a narrow range of orientations relative to the magnetic field direction, other regions being off-resonance. The exchange between these Xe atoms and the Xe atoms in other crystals oriented in other directions is very slow so the hole persists and the shape of the remainder of the powder pattern remains unchanged. In contrast, upon selective saturation of a narrow sliver of the "inside" Xe signal in the microcrystallites of silicalite, the hole does not persist; dynamics leads very quickly to a filling in at this frequency.

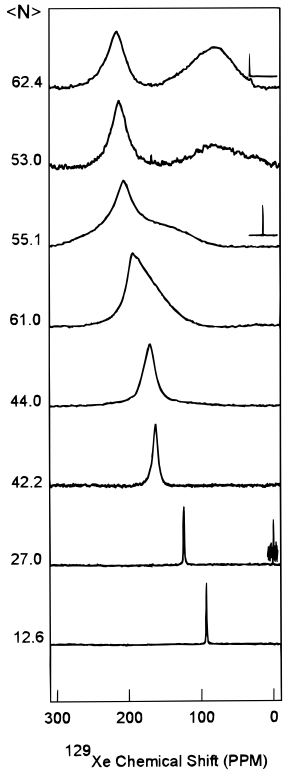

Figure 10. ^{129}Xe NMR spectra at 300 K of Xe in zeolite NaX at various loadings. For selected samples the observed overhead gas spectrum is also shown as an inset (see text). The calculated values of $\langle N \rangle_{Xe}$ (Xe atoms/unit cell), based on the density of the overhead gas, are indicated to the left of the figure.

We could not effect magnetization transfer experiments in the microcrystalline silicalite samples; inversion of either the gas peak or the occluded xenon resulted in complete averaging with the other peak before measurements could begin, indicating very fast exchange over a time much less than the ca. 500 μs DANTE pulse train. Direct full exchange between silicalite microcrystals can also occur if the solid exists as clumps of microcrystallites oriented in a variety of directions.

B. Xe in NaX. In Figure 10 are the first high-loading Xe spectra at room temperature in a faujasite. Cheung[50] and Ratcliffe and Ripmeester[15,51] have previously observed Xe at very high loading (10−12 Xe/supercage) in NaY and NaX at low temperatures. It was demonstrated that a sample of Xe in NaY, the highly siliceous version of faujasite, reached equilibrium at 77 K with nominal loading of 12 Xe atoms/supercage after 240 h, and showed already a small peak of solid bulk Xe.[15] At high overhead pressures of Xe gas we have achieved loadings as high as 8.5 Xe/supercage in NaX at room temperature; we were unable to prepare samples with high enough overhead pressures of Xe to observe the limiting chemical shift of Xe that could be reached when the zeolite is saturated at 12 Xe atoms per supercage. In Figure 10 the apparent Xe chemical shift increases significantly with increasing $\langle N \rangle_{\text{adsorbed Xe}}$ and then levels off at 220 ppm. Even though the occluded peak increases in chemical shift monotonically with loading, whereas the exchanging (broad) peak seems to change dramatically and behave independently with increased loading, the fact that the magnetization transfer experiments on Xe in NaX were not successful[52] indicates that exchange is occurring on the μs time scale. So one must suspect that the chemical shift of the occluded peak is reporting on more than reservoir IV.

C. Xe in CaA. For Xe in CaA at various loadings the apparent Xe chemical shift increases significantly with increas-

ing $\langle N \rangle_{adsorbed}$ and reaches 246 ppm at our maximum occupancy of about 8.5 Xe atoms/cage at room temperature.[53] The magnetization transfer experiments for a high loading sample of CaA indicates that complete exchange has occurred in 1 ms.[52] Therefore, the observed chemical shifts in high loading samples of CaA reported previously[53] probably should not be exclusively assigned to reservoir IV. Cheung reported the maximum capacity of CaA at 8 Xe atoms/cage at 144 K, with a corresponding Xe chemical shift of 299 ppm.[41] In our work,[53] at high overhead pressures of Xe gas we have achieved as high as 9 Xe/cage in CaA at 240 K.

In samples of Xe in CaA we have observed reservoir II xenon gas peaks that are homogeneously broadened compared to the gas peaks in NaA samples. We attribute this broadening to exchange of Xe atoms between interparticle gas and occluded environments. Analysis of the peak width and the magnetization transfer experiment corroborate the observed line broadening.[52] The occluded and interparticle xenon NMR signals in CaA samples are nominally separated by 10 kHz. Exchange between the two xenon reservoirs in CaA will begin to broaden the interparticle xenon gas NMR signal when the mean residence time for these xenon atoms is near 100 μs. We measured magnetization transfer between inter- and intracrystallite xenon CaA and found that the process is taking place on a 100 μs time scale for Xe in this zeolite. (See Figure 45 in ref 52.) We measured the coherence lifetimes of ^{129}Xe spins in CaA at low, medium, and high loadings. (See Figure 46 in ref 52.) The coherence lifetime is longest for the low loading sample and decreases with increased loading. The corresponding experiments for Xe in NaA reveal the same dependence. The Xe in CaA system illustrates Xe mobility intermediate between the very slow intracrystalline mobility observed for Xe within NaA[14] and the very fast intercrystalline mobility observed for Xe in 13X. In the latter the exchange rate is greater than the frequency separation between the Xe_n peaks and of the same order of magnitude as the frequency separation between the (intercrystallite) gas peak and the exchange-averaged occluded Xe peak, so that a weighted average chemical shift is observed for both the occluded Xe and the intercrystallite Xe gas in 13X. In the intermediate case of CaA the effect of the xenon mobility on the ^{129}Xe peak shape is to initiate exchange broadening, but the exchange (between xenon atoms inside the crystallites and those outside) is not fast enough to measurably shift the peaks.

IV. GCMC Simulations

A. Methods and Parameters. The grand canonical ensemble is appropriate for adsorption systems, in which the adsorbed phase is in equilibrium with the gas at some specified temperature. The use of a computer simulation allows us to calculate average macroscopic properties directly without having to explicitly calculate the partition function. Monte Carlo simulations in the grand canonical ensemble is now a widely used technique. We have carried out simulations at fixed (μ, V, and T). The grand canonical Monte Carlo (GCMC) method as applied in this work has been described in detail earlier,[17] so only a very brief account is given here. The silica framework $(SiO_2)_n$ is usually assumed to be neutral (purely covalent). The charge separation is introduced by the isomorphous substitution of Si by Al in which case counterions are required to balance the net negative charge of the framework. Cut-and-shifted Lennard-Jones (12-6) potentials were used to model the Xe−O interactions in Al-free silicalite, which is taken to be a strictly covalent structure. For the faujasites NaY and NaX, the Xe−O and Xe−Na interactions are modeled by Lennard-Jones potentials, and in addition, the polarization of Xe was considered as a separate contribution to the energy. The calculation of the nonpairwise-additive polarization energies and the effective charges used in these calculations have been described elsewhere.[26] The Xe−Xe potential used is of the Maitland−Smith form, as described in our previous simulations of Xe in NaA, fitted to the best available Xe−Xe potential of Aziz and Slaman.[17,54] The parameters used have been described earlier.[16,17,26] The simulation box is a unit cell with periodic boundary conditions imposed in three directions, using the minimum image convention, consistent with the cut-and-shifted potentials employed. The Markov chain is constructed using the Norman−Filinov method, that is, using three equally weighted types of moves, one involving displacement of a particle and two moves randomly chosen for either destruction or creation of a particle. The core of the program effects the creation/destruction and displacement of one atom at a time and calculates the associated energy change, ΔU in each case. This is used to continuously update the total configurational energy of the system, without having to recalculate every interaction at every step. For the very high-loading simulations we have improved the efficiency of simulations by using the cavity-biased particle insertion scheme, suggested by Mezei, that is more efficient at high densities than the standard Norman−Filinov scheme.[55]

We use in our simulation box the actual coordinates of the framework atoms and charge-balancing cations derived from X-ray diffraction data. For silicalite, the all-Si version of zeolite ZSM-5, we use the coordinates that have been determined by van Koningsveld et al.[56] Crystallographic and solid-state NMR studies have shown two distinct forms of silicalite: orthorhombic, found at high temperature and a low-temperature monoclinic form.[57,58] For unloaded silicalite the transition occurs at 340 K. We use the coordinates from the calcined monoclinic form for our simulations which will be compared with data at or below room temperature. The solid state ^{29}Si NMR spectrum of an extremely pure and very highly crystalline form of silicalite shows 21 of the 24 types of Si sites consistent with the crystallographic symmetry of the monoclinic form (whereas the orthorhombic form should have only 12 types of Si sites).[59] We carried out GCMC simulations in both the orthorhombic and monoclinic forms, but only the results from the monoclinic form are shown here for comparison with experiment.

The crystallographic unit cell of faujasite has the composition $Na_xAl_xSi_{192-x}O_{384}$, where $96 \geq x \geq 0$ and the two variants X and Y differ only in their Si/Al ratios, X having a lower Si/Al ratio (and hence more cations) than Y. In the present study we have used zeolite NaX with $x = 88$. There are a number of X-ray diffraction results in the literature for dehydrated NaY at various Si/Al ratios, and these yield coordinates for the framework atoms differing by 0.5−0.7%.[60−64] Na^+ ion sites have been identified (using the standard labels for extraframework cation sites[65,66]): I, I′, U, U′, II, III, and III′. Primes designate positions close to the classical ion positions. I is at the center of the hexagonal prism; U is at the center of the sodalite cage. Classical sites II and III are in the supercage, located symmetrically above the plane of the 6-ring and above the 4-ring of the sodalite unit, respectively. Several structures have been reported for NaX,[64,67−69] differing in the precise locations of Na(III or III′) ions. For our NaX simulation box, we have adopted the coordinates reported for $Na_{88}Al_{88}Si_{104}O_{384}$ (Si/Al = 1.18) refined in space group $Fd3$ by Olson.[68] For NaY we have adopted the coordinates reported for Si/Al = 2.37 from the work of Mortier.[61] Zeolite Y was given a unit cell length of 24.786 Å and zeolite X a unit cell length of 25.099 Å. The framework was represented by the $Fd3m$ space group

TABLE 1. Potential Energy Parameters Used in the GCMC Simulations

V(Xe−O)	V_{LJ} (set I)	V_{LJ} (set II)
r_0, Å	3.443	3.70
ϵ/k_B, K	168	130

with the origin at the center of a β cage. This representation places a large cavity at the center of the unit cell and each unit cell contains eight large cavities. For the purpose of calculation of the polarization energy, we could have used one of the suggested distributions of the Si and Al atoms in the framework based on the position and shape of the five Si(*n*Al) bands in the ^{29}Si MAS NMR spectrum of NaY and NaX. The spectrum is a superposition of many components arising from the multiple local environments for a Si atom, the local environments differing in the number and types of first and second-shell Al substituents. For example, Thomas, Klinowski, and Fyfe have suggested a series of Si, Al ordering schemes based on the ^{29}Si spectra, crystal symmetry and minimizing electrostatic interaction energies.[71,72] More recently, Melchior et al. have used the band positions and heterogeneous band shapes to arrive at a distribution of D6R subunits with a specific number of Al atoms.[73] Instead we represent Si and Al atoms with an average T atom with partial charge weighted according to the Si/Al ratio. We placed the ions, 88 Na^+ for our experimental sample of NaX, and 48 Na^+ as a representative for NaY, as follows: All the type II (32e sites) are filled for both zeolite NaY and NaX. This is consistent with the site II occupancies very close to 32 in various reported structures with Si/Al = 1.18−4.74.[60−64,67,68] Structures show both sites I and I′ are partially occupied in NaY, while I′ is nearly filled in NaX.[64,68] For simplicity, all the sites of type I (16c) are filled in the NaY simulation box, and all sites I′(32e) are filled in zeolite NaX. The last 24 Na^+ ions in NaX partially occupy the site III′ window positions. Some structures place these Na^+ close to the plane of the 12-ring window, only Hseu[67] finds Na(III) binding four oxygens, two of which are in the 12-ring window. The structure reported by Olson[68] has less symmetry in the positions of the Na(III), although quite close to those given by Eddy.[64] We choose the symmetrical one of the Olson (III′) basis coordinates. For a simulation box that can be propagated periodically, we placed the site III Na^+ ions such that each 12-ring window has one Na^+ ion in a site III′. The remaining 8 Na^+ ions were randomly placed such that each supercage has two windows with 2 Na^+ ions and two windows with one Na^+ ion. These locations were not strictly optimized so as to minimize the cation repulsive energy in 36 supercages + 36 β cages. Thus, the arrangement is more similar to the disordered arrangements of Na(III) ions in NaX zeolite. The full coordinates of the unit cells are generated by applying 192 symmetry operations to the basis set of coordinates given in ref 68. The polarization energies were calculated for a Xe atom in the central supercage surrounded by 35 supercages and 36 β cages, using a fine grid of coordinates for the Xe atom (60 × 60 × 60, 0.2091 Å grid in *x*, *y*, and *z* in NaX, 0.206 55 Å grid in NaY). A table-look-up with interpolation was used during the simulations, just as described elsewhere.[26] The partial charge used for Na, Si, and Al is the same used previously for NaA, CaA, and $Ca_xNa_{12-2x}A$.[26] The charge of the "typical" T atom (Si or Al) in NaY or NaX is taken to be an average charge according to the proper weights based on the Si/Al ratio. The partial charge on the O atoms is calculated so that the entire system can be neutral. The Lennard-Jones potential used in the faujasites NaY and NaX in the present work for the interaction between Xe and the O atoms is the same one, unchanged, that we have used for Xe in NaA, CaA, and $Ca_xNa_{12-2x}A$ in ref 26. This is given in Table 1 as parameter set I. The same V(Xe−Na) as was used in ref 26 is used in all calculations in the present work. This V_{LJ}(Xe−O) (parameter set I) has not been adjusted in any way to agree with any experimental data in silicalite or with the faujasites. We also wanted to test an effective 2-body function V_{LJ}(Xe−O) to approximate the Pellenq−Nicholson Xe−zeolite potential (PN1), which had been constructed from 2-body parts for Xe−O and Xe−Si augmented with 3-body terms.[74] We have constructed an effective V_{LJ}(Xe−O) to approximate the PN1 potential (parameter set II in Table 1).

We use here, without modification, the Xe shielding functions for Xe−O and Xe−Na that have been derived from ab initio calculations using fragments of the NaA, KA and CaA α cages.[25] We use the same Xe−Xe shielding function as we have used previously for Xe in the gas phase[21] and for simulations of Xe in zeolite NaA, KA, CaA, and Ca_x-$Na_{12-2x}A$.[16,17,26] The GCMC simulations provide the adsorption isotherms and the average chemical shift for Xe in the adsorbed phase.

We consider Xe in silicalite. This is a test of the validity of the partitioning of our shielding function into Xe−O and Xe−Na from the total shieldings calculated in the presence of various fragments of the zeolite cage. Unlike other zeolites, in silicalite, there can be no ambiguous compensation between the two Xe-lattice contributions, since only the Xe−O shielding function contributes. Furthermore, it would be interesting to test the transferability of the Lennard-Jones potential function for Xe−O interactions that was used in Al-containing zeolites such as NaY and NaX, CaA, NaA, and KA (where polarization of the Xe augments the Lennard-Jones Xe−O and Xe-cation potentials) to an all-silica framework such as silicalite, which has quite different structure (mostly channels, rather than cages) from the faujasites or A zeolites.

B. GCMC Results for Xe in Silicalite. The results of the GCMC simulations of Xe in silicalite are shown in Figures 11−13. In this work, the adsorption isotherm is provided by the density of the Xe gas in equilibrium with the Xe adsorbed in silicalite obtained from the chemical shift of the Xe in the overhead gas, as described in the Experimental Section. We show in Figure 11, the experimental adsorption isotherm reported by Dybowski et al. at 300 K,[75] which agrees reasonably well with our values (>) in Figure 11. We find that including induction terms in silicalite has only a small effect on the predicted adsorption isotherm. Using the same Lennard-Jones V(Xe−O) function (parameter set I) as were used for Xe in NaA and in $Ca_xNa_{12-2x}A$[26]; the simulations produced greater adsorption in silicalite than is found experimentally at room temperature. On the other hand, GCMC simulations using parameter set II leads to results in excellent agreement with the adsorption isotherm calculated by Pellenq and Nicholson[42] using the PN1 potential. GCMC simulations using our parameter set II (+ and ×) provides good agreement with the experimental adsorption isotherm at 300 K from this present work, at 295 K from Dybowski et al.[75] It also provides reasonably good agreement with the experimental data at 195 K from Chen[45] and in the range 121−296 K from Bülow et al.[76] Using parameter set II leads to a maximum loading of 16.5, close to experiment. It should be noted that a maximum occupancy of about 20 Xe atoms/unit cell had been reported at 144 K by Cheung,[41] whereas the adsorption isotherm at 195 K reported by Chen[45] corresponds to a maximum loading at 195 K of only 16 Xe atoms/unit cell, and Bülow et al. report a similar maximum (17 Xe atoms/unit cell) from adsorption measurements over the range 121−296 K.[76]

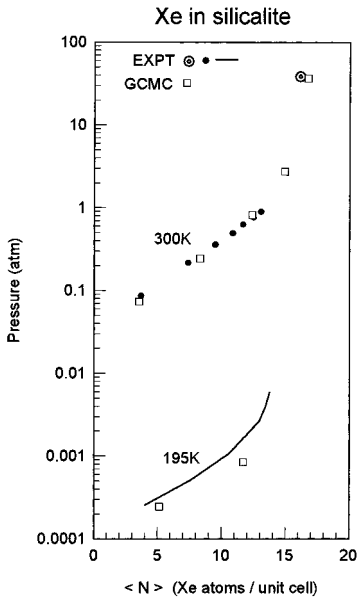

Figure 11. Adsorption isotherms from GCMC simulations for Xe in silicalite at 300 and 195 K using L−J parameter set II without induction energy terms (□) are shown at 300 K and at 195 K. These are compared with experimental data (●) from Dybowski et al. at 295 K,[75] (⊙) from this work at 300 K, and the experimental data (—) from Chen at 195 K.[45]

We have compared the experimental average ^{129}Xe NMR chemical shifts in the adsorbed phase in silicalite (shown in Figure 5) with some ^{129}Xe chemical shifts reported in the literature for silicalite at 295 K.[75] We find that the apparent ^{129}Xe chemical shifts reported for the microcrystalline samples used by Dybowski et al.[75] are in good agreement with those found in microcrystalline samples in this work. They are, of course, not the ones that reflect the actual chemical shifts of the adsorbed phase except at very low loading of Xe. The ^{129}Xe chemical shifts measured in the large crystals of silicalite and in the low loading samples are the ones that should be compared with the GCMC average values found at various xenon loadings $\langle N \rangle_{Xe}$. Figure 12 shows that we do obtain excellent agreement with GCMC simulations using V_{LJ}(Xe−O) with parameter set II.

We show in Figure 13 the predicted temperature dependence of the average ^{129}Xe chemical shifts in silicalite. In this figure the results of GCMC simulations at 144 K are compared with those at 300 K. Using parameter set II, the predicted 144 and 300 K chemical shift curves converge to the same value at the intersection point which occurs at a loading of 6 Xe atoms/unit cell. Below this, chemical shifts at the same loading are greater at lower temperatures. Included in Figure 13 for comparison are the experimental chemical shifts reported by Cheung at 144 K.[41] The GCMC simulations in silicalite predict at high loading smaller Xe chemical shifts at lower temperatures, inconsistent with the data in Figure 6. The pseudo-isotropic chemical shifts that are obtained from the singularity points of the powder patterns at the three temperatures [δ_{iso}(240 K) = 183.5 ppm, δ_{iso}(270 K) = 180.8 ppm, and δ_{iso}(300 K) = 176.9 ppm] do not change in the direction predicted by the GCMC simulations at high loadings.

These are the first GCMC simulations of Xe chemical shifts in silicalite. There has been a GCMC simulation of Xe in silicalite by Pellenq and Nicholson,[42] which was mainly concerned with the adsorption isotherm and the isosteric heat. There have been molecular dynamics simulations in silicalite,[43,44,46] all of which were concerned with the diffusion coefficients of Xe inside silicalite.

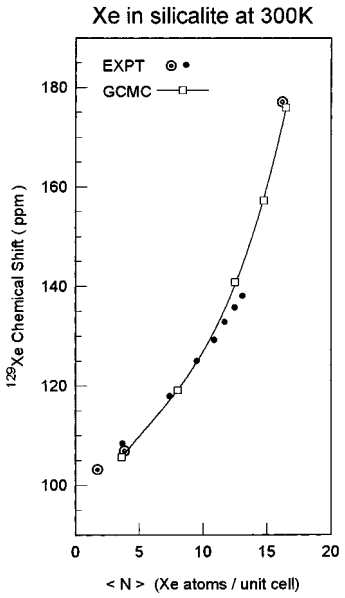

Figure 12. Average ^{129}Xe chemical shifts from the GCMC simulations of Xe in silicalite at 300 K: (− □ −) using parameter set II in V_{LJ}-(Xe−O). These are compared with experimental data (⊙) from this work, at 300 K, and (●) in silicalite at 295 K.[75]

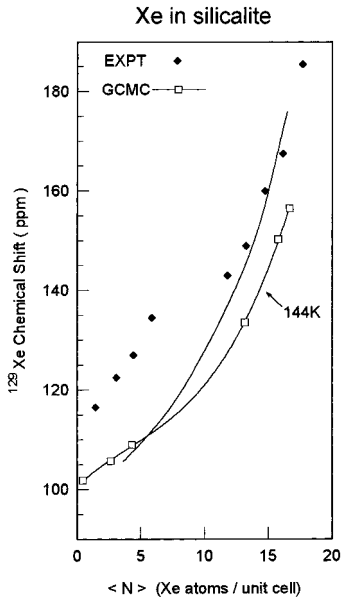

Figure 13. Average ^{129}Xe chemical shifts at 144 K from the GCMC simulations of Xe in silicalite, (− □ −) using parameter set II in V_{LJ}-(Xe−O). These are compared with experimental data for Xe in silicalite (◆) from Cheung[41] at 144 K. Also shown for comparison are the GCMC simulations at 300 K using parameter set II (—) that are shown in Figure 12.

C. GCMC Results for Xe in NaY and NaX. Since the Si/Al ratio in our NaX sample (Linde 13X) has been determined to be 1.18, we use this Si/Al ratio in our simulation box as a representative of NaX for comparisons with experiments. We also carried out GCMC simulations in NaY using Si/Al = 3.0 as a typical sample. We used the same Lennard-Jones parameters and the same partial charges as were used for Xe in NaA and in $Ca_xNa_{12-2x}A$.[26] In Figure 14, the GCMC results for NaX are compared with those for NaY. We find that only by including induction terms can we reproduce the general qualitative trend of greater adsorption in NaX compared to NaY. The generally greater adsorption of Xe by zeolites of higher (Al + cation) content has been observed experimentally in several studies.[9,10] Using Lennard-Jones V(Xe−O) and V(Xe−

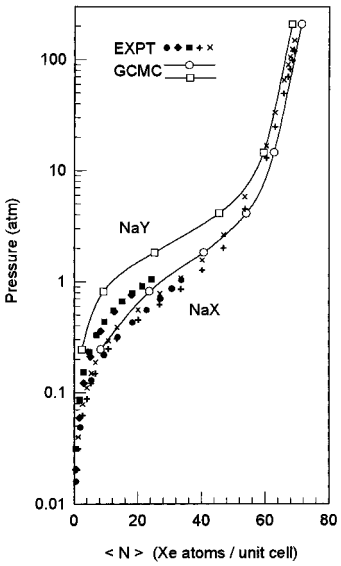

Figure 14. Adsorption isotherms (○) from GCMC simulations of Xe in zeolite NaX (Si/Al = 1.18), and (□) in NaY (Si/Al = 3.00). These are compared with experimental data (●) in NaX (Si/Al = 1.23) at 295 K from Liu,[78] in NaX (Si/Al = 1.18) from Fomkin[77] at (+) 296 K (×) 303 K, and in NaY from Liu et al. (Si/Al = 2.70, 2.49) (■, ◆).

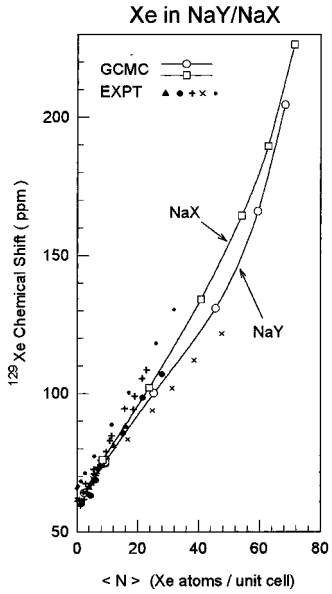

Figure 15. Average ^{129}Xe chemical shifts at 300 K from the GCMC simulations of Xe (□) in NaX (Si/Al = 1.18), and (○) in NaY (Si/Al = 3.00) are compared. These simulations are compared with experimental data (•) in NaX (Si/Al = 1.23) at 293 K from Liu,[10] (●) in NaY (Si/Al = 2.49) at 293 K from Liu,[10] (▲) in NaY (Si/Al = 2.4) at 298 K from Boddenberg et al.,[79] and (×) in NaY (Si/Al = 160) at 300 K from Gupta et al.[80] Also shown are (+) the experimental data in NaY at various Si/Al ratios ranging from 1.28 to 54.2, at 298 K from Ito et al.[4]

Na) functions alone do not permit the differences in the adsorption isotherms that arise upon decreasing the Si/Al ratio to be reproduced. The predicted adsorption isotherm in Figure 14 may be compared with the adsorption isotherms of Xe in NaX (Si/Al = 1.18) that have been measured by Fomkin at 296 and 303 K[77] and with the adsorption isotherms of Xe in NaX (Si/Al = 1.23) that have been measured by Liu et al. at 295 K.[78] The predicted adsorption isotherm for NaY in Figure 14 can be compared with the experimental adsorption isotherms reported by Liu et al.[78] for Xe in NaY (Si/Al = 2.49 and 2.70). The agreement between the GCMC results and the experimental adsorption isotherms in NaX is good. The comparison of the predicted relation between the adsorption isotherms for NaY and NaX with that obtained experimentally in the same laboratory (Liu et al.) is also good. The experimental results are in excellent agreement with one another and the GCMC results agree reasonably well with these experimental data, although a bit weaker adsorption is simulated than the actual experiments. There is a lot of scatter in the adsorption isotherm that could be obtained at high loading by observing the Xe chemical shift in the overhead gas in equilibrium with the Xe adsorbed in the NaX zeolite, so we have not included this in Figure 14. The maximum loading found in the GCMC simulations in the present work, 8.55 and 8.9 Xe/supercage, respectively, in NaY and NaX at room temperature, is about the same as the highest loadings achieved in the experimental adsorption isotherms of Fomkin,[77] and about the same as the maximum loadings we had been able to achieve at room temperature. However, the simulations do not achieve loadings as high as the 12 Xe atoms/supercage that had been reported at 77 K by Ratcliffe and Ripmeester;[15] we get only 10.7 Xe atoms/supercage at this temperature. We do get a maximum loading of 10.0 Xe atoms/supercage at 144 K, the same as that reported by Cheung et al. at this temperature.[50]

While the Xe adsorption isotherms are markedly dependent on the Si/Al ratio in faujasites, the average ^{129}Xe chemical shifts are somewhat less sensitive to the Si/Al ratio. Initially, the experimental chemical shifts at a given loading in NaY and NaX were found to be comparable, new, all the ^{129}Xe chemical shifts vs $\langle N \rangle_{Xe}$ (at loadings up to 3 Xe per cavity) in zeolite NaY of varying Si/Al ratios had been found by Ito and Fraissard to fall on the same line when the Si/Al ratios varied from 1.35 up to 54.2.[4] Subsequent work by Liu et al.,[10] revealed a systematic change in the ^{129}Xe chemical shift at the zero-loading limit and also a systematic change in the slope of the dependence of the chemical shift on $\langle N \rangle_{Xe}$.

It is worthwhile to test the sensitivity of the ^{129}Xe chemical shift to the number of charge-balancing cations in NaX/NaY by GCMC simulations. As a model for NaY we have chosen a zeolite with Si/Al = 3.0 in order to compare with the literature values. In Figure 15 the GCMC average chemical shifts for Xe in NaY and NaX are compared with each other. We find a small but systematic difference between the average Xe chemical shift for Xe in faujasites with Si/Al ratios 3.0 and 1.18 at low loadings and the curve for Xe chemical shifts in NaX and in NaY deviate significantly from each other at intermediate loadings.

In Figure 15 we compare the predicted average Xe chemical shifts from GCMC simulations in NaY (Si/Al = 3.0) and NaX (Si/Al = 1.18) with the experimental data in NaX and NaY previously reported by several workers: Liu et al. (Si/Al = 1.23, 2.49, 2.70),[10] Boddenberg et al. (Si/Al = 2.4),[79] Ito and Fraissard (Si/Al = 1.35−54.2),[4] and Gupta et al. (Si/Al = 160).[80] Except for the earliest data of Ito and Fraissard, the trends are quite clear: ^{129}Xe chemical shifts are greater for the faujasites with higher Al content. We find excellent agreement in trends between the room temperature GCMC average chemical shifts and the experimental chemical shifts. The agreement of the GCMC simulations with magnitudes of experimental data is reasonably good despite adopting the same parameters for the V_{LJ}(Xe−O) and V_{LJ}(Xe−Na) and the same partial charges for the induction terms, *without change* from those which had been used for $Ca_0Na_{12}A$, $Ca_1Na_{10}A$, Ca_2Na_8A, and Ca_3Na_6A.[26]

One of the advantages in having carried out experiments in the model system Xe_n in NaA is that each peak observed corresponds to a known unchanging number of Xe atoms in the cage, even as the temperature is varied. Thus, we were

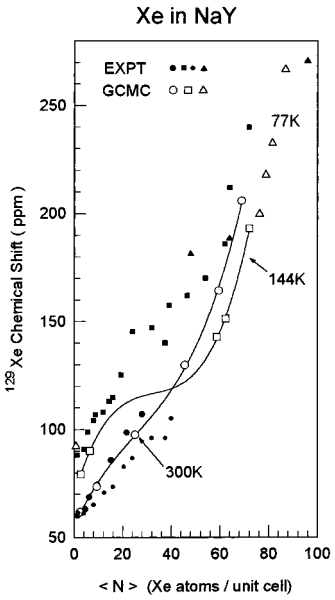

Figure 16. Temperature dependence of the average ^{129}Xe chemical shifts in NaY: The GCMC simulations of Xe in zeolite NaY (Si/Al = 3.0), (− ○ −) at 300 K, (− □ −) at 144 K, and (△) at 77 K are shown. Experimental data (●) at 293 K in NaY (Si/Al = 2.49 and 2.70), from Liu et al.[10] are shown to represent most of the room-temperature data plotted in Figure 15. These are compared with the experimental data in NaY (Si/Al = 2.62) from Cheung,[50] (•) at 293 K and (■) at 144 K. Also shown are experimental data (▲) in NaY (Si/Al = 2.70) at 77 K from Ripmeester.[15]

able to definitely establish the different temperature behaviors of the Xe chemical shift in low occupancy cages in contrast to high occupancy cages.[14] And these temperature behavior has been reproduced very well by the GCMC simulations.[17] Now we can consider the temperature dependence of the Xe chemical shift in an open network zeolite. The temperature dependence of the average Xe chemical shifts obtained from GCMC simulations at 300, 144, and 77 K in NaY (Si/Al = 3.0) are shown in Figure 16. We find that in this zeolite the intersection point between the average shifts at 300 K and those at 144 K occurs at an intermediate loading of about 42 Xe atoms/unit cell. At loadings lower than this, the behavior of the temperature dependence is like that of the Xe_1 peak in NaA. On the other hand, at much higher loadings, the chemical shift increases with increasing temperature, the behavior we had observed for the Xe_6, Xe_7, and Xe_8 peaks in NaA. Thus, our simple model system, Xe_n in NaY, provides us with the understanding of the temperature dependence of chemical shifts in variable loading samples such as Xe under fast exchange in NaY. The GCMC simulations are compared with the experimental data in NaY reported by Cheung for 293 and 144 K and with the data reported by Ratcliffe and Ripmeester at 77 K.[15] To reduce clutter, only the Liu data at room temperature[10] are included in Figure 15 to compare with the data from Cheung.[50] We find that Cheung's data at 293 K do not agree with the room temperature data reported by other workers; nevertheless, the Cheung data provide experimental results at two different temperatures in the same sample and should serve as an example of the temperature-dependent behavior at low loadings. The GCMC simulations reproduce the experimentally observed increase of ^{129}Xe chemical shift with decreasing temperature *at a given* $\langle N \rangle_{Xe}$. We see in Figure 16 that the trends in the relative shifts in going from room temperature to 144 K are well reproduced, although quantitative agreement at the lower temperatures is not obtained with Cheung's data at 144 K and Ripmeester's data at 77 K.

Additional information available from the GCMC simulations, such as the Henry's law constants, may be compared with experiment. For Xe in silicalite two experimental values of Henry's law constant have been reported: $k_H = 2.2 \times 10^{-2}$ mmol/(g Pa) at 195 K and $k_H = 2.25 \times 10^{-4}$ mmol/(g Pa) at 273 K.[45] Pellenq and Nicholson's PN1 potential yielded $k_H = 3.74 \times 10^{-2}$ and 2.90×10^{-4} mmol/(g Pa) at 195 and 273 K, respectively,[42] whereas our GCMC simulations using parameter set II in the present work, lead to 3.66×10^{-2} and 2.44×10^{-4} mmol/(g Pa) at 195 and 273 K, respectively, in good agreement with the results of Pellenq and Nicholson. GCMC simulations have been carried out independently by McCormick and his group for Xe in NaY using a chemical shift that has been parametrized to agree with experiment.[80] In our work, on the other hand, we have used the same chemical shift functions, based on ab initio calculations, for Xe−O, Xe−Na, and Xe−Xe interactions as we have used from the beginning, to interpret the observations for Xe in NaA, Xe + Ar in NaA, Xe + Kr in NaA, Xe in $Ca_xNa_{12-2x}A$, and in the present work. Molecular dynamics simulations of the diffusion of Xe in NaY have been carried out by Yashonath[81] and by Mosell et al.[82]

V. Discussion

A. Limiting Case Behavior of Xe NMR Spectra in Zeolites. In discussing the NMR spectra of Xe in various open network zeolite types, where the Xe is in sufficiently fast exchange to present only a single peak for the adsorbed Xe atoms at room temperature, it would be helpful to consider various limiting cases.

Case A. Case in which no more than a single Xe atom is immobilized in a zeolite cage at low temperatures. For the "inside" peak; each unique low-energy adsorption site will have a characteristic anisotropic Xe shielding tensor. The observed line shape will be a convolution of the relative probabilities of the various orientations of the crystallite with respect to the magnetic field (which is well-known for a powder), the shielding tensor components, and the populations of the adsorption sites. There is no reported example of this in a zeolite; shielding tensors of immobilized Xe in a small clathrate cavities have been reported, however.[83]

Case B. Case in which there is fast intracage exchange as well as a *slow* intercage exchange. For the "inside" peak, a single Xe atom inside a cage has a single average shielding tensor which is a mathematical average over all configurations of the individual second-rank tensors for individual configurations. This average is a second-rank tensor, which we will call an "average shielding tensor" due to rapid intracage exchange. The Xe atom samples not only the different lowest energy adsorption sites but all positions within the cage, weighted according to the Boltzmann factor. Since a single Xe atom samples only one cage at a given orientation of the crystallite in the magnetic field, it reports on the average shielding tensor for that orientation. If the cage is spherical, or of symmetry *T*, T_h, T_d, *O*, O_h, or K_h, then the average shielding would be given by the isotropic shielding value associated with the average shielding tensor, independent of the orientation,[84] but even the α cages in A-type zeolites which have cubic frameworks are anisotropic. For example, NaA has a single Na^+ ion coordinated to a 4-ring, thus imposing a unique direction. There are other more subtle deviations from strictly cubic symmetry. The Na^+ ions that sit in the plane of the 8-ring windows are not in the center of the ring, but rather are off-center. As the orientation of the cage with respect to the magnetic field is changed, the anisotropic average shielding tensor along the magnetic field direction is traced out. For a collection of cages, the distribution

of orientations leads to a powder pattern, which is characteristic of the average shielding tensor for Xe in the cage, but not for the shielding tensor for a Xe atom in an adsorption site. When there is a fixed number of atoms of Xe in the cage, each configuration of the Xe_n in the α cage has characteristic shielding tensors for each of the *n* Xe atoms. The average shielding tensor is an average over all the shielding tensors associated with all *n* atoms in a configuration, averaged over all possible configurations, each weighted by the Boltzmann factor for the configuration. The intracage average depends on temperature because the weighting factors do. (But, at different temperatures, the configurations change and the *n* shielding tensors for a particular configuration of Xe_n also change.)

For the "outside" (reservoir II) peak, the chemical shift observed for this sharp peak is the true chemical shift for the overhead bulk gas (reservoir I), except for the bulk susceptibility contribution from the zeolite crystallites, since the exchange with the "inside" (reservoir IV) Xe atoms is slow.

A typical example for this case Xe_n in NaA.[14] The powder pattern should change with *n*. For a given Xe_n, it should change with temperature. In this case, however, the anisotropy of the α cage is not very great, so the observed powder pattern characteristic of each Xe_n is only about 10 ppm wide and independent of the average loading. We had previously found that it is possible to "burn" a hole as narrow as 1 ppm in one of the broad lines in a Xe/NaA spectrum by using a selective DANTE pulse sequence. Carr−Purcell−Meiboom−Gill (CPMG) T_2 experiments on several different samples of Xe in zeolite NaA have yielded relaxation times of 15−40 ms, indicating limiting line-widths in the range of ∼10−20 Hz.[85] This evidence suggested that the broad lines are a superposition of a large number of narrow resonances with a range of chemical shifts. We believe that the nature of this superposition is that of a powder pattern, which should be reduced to a narrow line by magic angle spinning. Indeed, we have found for our Xe in zeolite NaA samples, that even slow (∼2 kHz) sample spinning caused a remarkable narrowing of the ∼1 kHz experimental line widths, down to ∼100 Hz.[85] Xe in the clathrasil decadodecasil-3R provides another example. Exchange cannot occur in the fully loaded clathrasil. When the cages are fully occupied with 2 Xe atoms each, a powder pattern characteristic of a nearly axially symmetric shielding tensor with anisotropy of ca. 75 ppm is observed for the adsorbed phase even at room temperature and this powder pattern narrows down to about 2−3 ppm upon magic angle spinning.[86,87]

Case C. Case in which there is fast intracage exchange as well as fast intercage exchange and large crystallites. For the "inside" peak, because of the fast intercage exchange, the occupancy of each cage is not a constant; there is a distribution of occupancies. Also, if there is more than one kind of cage or channel (as in silicalite), there is also a wider variety of shielding environments. Thus, if the exchange is rapid between all channels at the temperature of the experiment, a single Xe atom samples all the environments (various occupancies of sinusoidal and straight channels and intersections) within a crystallite and reports a loading-dependent resonance frequency which depends on the orientation of that crystallite in the magnetic field. Since the average shielding tensor is an average over the configurations of various numbers of Xe in sinusoidal channels, straight channels, and intersections, the powder pattern should change with loading as well as temperature.

For the "outside" peak, the gas peak is very narrow, typical of bulk gas with a relatively long relaxation time, with a chemical shift characteristic of the density of the bulk gas. If the crystals are large enough, only a minute fraction of the "inside" Xe atoms near the channel exits are capable of exchanging with the gas between the crystals.

We have observed this behavior for Xe in large crystals of silicalite. Exchange is slow in the fully loaded Xe in silicalite crystal, so that the powder pattern could be observed, as seen in Figures 3 and 6. At the lower temperature, the isotropic shielding moves to greater deshielding (higher chemical shift) and the shielding anisotropy becomes even more pronounced than at room temperature. The spectra in Figure 3 are of very high-loading samples (believed to be at saturation). The magnetization transfer studies of Xe in the large silicalite crystals tell us that, even though slow, exchange *is* taking place, although the exchange is probably not a simple two-site exchange since a large fraction of the "inside" Xe (reservoir IV) do not participate in this exchange. But, when the unit cell is completely full, how can there be any exchange at all between sinusoidal and straight channels? The nature of this averaging may be similar to that described by Kärger et al. as single-file diffusion.[88] Are the Xe atoms moving in a correlated way pushing one out through a channel exit as another one comes in from the outside? Loading-dependent anisotropies have also been observed in molecular sieves with one-dimensional pore structure such as ALPO-5, ALPO-11, VPI-5, ALPO-8, ZSM-12, and SSZ-24.[34] In ALPO-11 the channel is a cylinder with a chain of single-occupancy adsorption sites, four per unit cell. The small cross section of the channels in ALPO-11 permits an analysis in terms of a small number of ^{129}Xe sites, (with zero, one, or two Xe neighbors) each with a characteristic shielding tensor.[38] Xe atoms in unconnected straight channels such as in ALPO-11 are thought to diffuse by single-file diffusion.[88]

Case D. Case has fast intracage exchange, fast intercage exchange, and medium to fast inside−outside exchange. For the "inside" (reservoir IV/III) peak, when a significant fraction of the Xe atoms inside are capable of exchanging with the Xe outside, this would result in a collapsed powder pattern. The centroid of the peak is no longer characteristic of the average shielding of "inside" Xe atoms but is partly weighted by exchange with the Xe atoms near or on the outside surface, that is, the centroid will be somewhere between the bulk gas Xe chemical shift and the "inside" Xe chemical shift.

For the "outside" (reservoir II) peak, similarly, the peak arising from the Xe atoms between the crystallites will no longer be a sharp peak having a characteristic chemical shift of the bulk gas (after correction for the anisotropy of the magnetic susceptibility of the zeolite). Rather it will be more spread out and its centroid will be at a chemical shift weighted by exchange with the "inside" Xe atoms. Of the Xe atoms found between crystallites, some may be adsorbed on the outer surface. The smaller the crystallites, the larger will be the population of Xe in reservoir III and the larger the total outer surface. The Xe between the crystallites will be exchanging with atoms adsorbed on the outer surface and with atoms in reservoir III. The apparent gas chemical shift will not be the same as in the overhead bulk gas.

We observe this case at various intermediate and high loadings of xenon in the small crystallites of silicalite in Figure 4, and also in all but the lowest loading of Xe in NaX in Figure 10. The spectra of Xe in CaA[53] fall in-between the high-loading and low-loading behavior in these two systems.

An extreme limit of case D is when all the "inside" Xe atoms are capable of exchanging with the outside. Only an average chemical shift is observed; the peak is very sharp since it is under fast exchange (that is, a single Xe atom samples the inside of many crystallites at various orientations with respect to the

field and reports a single average frequency). This can happen in the zero-loading limit for a zeolite with a fairly open network. In zeolites with open networks, the diffusion rate increases with decreasing loading. Since intra- and intercrystallite diffusion is fast at low loadings, there is only one average chemical shift for all the atoms in reservoirs II and III and there is essentially no reservoir IV. Nearly all the Xe atoms are inside, so the chemical shift of the observed peak is very close to that characteristic of the "inside" average chemical shift. A clear example is the peak observed for the lowest loadings of Xe in silicalite, $\langle N \rangle_{Xe} < 4$ Xe atoms/unit cell, in the lower part of Figure 4. We also find this for the spectrum at the lowest loading of Xe in NaX in Figure 10.

The morphology of the crystalline material also affects the range of average chemical shifts observed, that is, the line width. In the case of silicalite, it can be seen in Figure 4 that the peak at highest chemical shift (reservoir IV) is not very wide (although wider than any Xe_n peak in NaA), despite the more anisotropic internal surface in silicalite compared to NaA. This comes about because in these silicalite samples the crystallites were clumped together, so that unit cells in many different orientations could be explored by a single Xe atom without going outside. This averaging over various orientations collapses the powder pattern. At low loadings a single Xe atom averages over several clumps of crystallites, leading to a narrow chemical shift range, a much narrower peak than that for Xe at a comparable loading in NaX. Since it is known that the intracrystallite diffusion rate for Xe decreases with increasing loading for silicalite (also for Xe in zeolite NaX),[89] as loading is increased, intracrystalline diffusion becomes slower, a range of chemical shifts is observed since a single Xe atom may average over one clump of crystals at best, and not all clumps are identical. The peak for the "inside" Xe atoms in Figure 4 starts out very narrow and becomes increasingly broader since exchange plays an important role in the line shapes.

Let us now consider the peak corresponding to the "outside" Xe, that is, the Xe between the crystallites (reservoir II). The "outside" peak arises from the Xe atoms in the intercrystalline void spaces. There is a distribution of such void space environments. We have seen already that at the lowest loadings, inside and outside environments are sampled by a Xe atom leading to a single very narrow peak weighted heavily by the "inside" environment since there is very little Xe in the gas phase. As the total Xe in the sample is increased, a gas peak is observed separating from the "inside" peak. The "outside" peak starts out fairly narrow at low loading, and starts to appear separate from the "inside" peak at a loading where crystallite saturation occurs and there is sufficient density of gas outside the crystallites. As long as the density of gas is low enough that the diffusion in the gas phase from one intercrystalline void to another is fast, only the average of the disparate void environments is reported, thus a narrow "outside" peak is observed. At some intermediate loading, while the "inside" peak remains fairly narrow, the "outside" peak becomes very broad. At this point, the gas density is high enough that diffusion from one void environment to another is slow and we see the dispersion of chemical shifts characteristic of the broad distribution of void types. As the total number of Xe atoms in the sample is increased, the apparent chemical shift of the "outside" peak changes monotonically toward that observed in the overhead gas (reservoir IV). At low gas densities, the ratio of populations of reservoirs II/III starts to increase and the apparent chemical shift from these reservoirs moves toward the overhead gas. As the total Xe in the sample is increased further, the ratio of reservoirs II/III increases further, the fraction of the exchanging population that is outside becomes larger (since the Xe gas density required to stay in equilibrium with the adsorbed phase is greater) while the fraction of the exchanging population that is inside becomes smaller. When the total Xe in the sample is increased further after saturation is reached, the chemical shift of the "inside" peak no longer changes; the relative intensity of the reservoir II peak grows and its centroid approaches the chemical shift of the overhead bulk gas. Once the pores of the silicalite saturate, the xenon concentration only increases in the intercrystalline reservoir and the weighted average chemical shift is shifted toward that of the overhead gas.

It has previously been observed that the apparent "inside" Xe chemical shift in a loose zeolite powder, where the crystallite-gas and intercrystallite Xe exchange are fast, is different from that when the intercrystallite distance is vastly reduced, as in a die compressed pellet, where most of the free Xe gas is too far from the crystallite surface for fast exchange. Effects of packing and compression of zeolite powders have been discussed by Chen and Fraissard,[90] by Tway and Apple,[91] and by Ripmeester and Ratcliffe.[92] In the example given by Ripmeester et al., the ^{129}Xe chemical shift in the compressed pellet is greater by 4.7 ppm than that in a loose powder.[92] The larger fraction of time xenon spends outside of the zeolite during the intercrystallite averaging, the smaller the observed chemical shift. The compressed pellet provides a more accurate ^{129}Xe chemical shift for the "inside" Xe atoms since the intercrystallite volume is greatly reduced by die-compression.

B. Powder Pattern Spectra. Under what conditions should we expect to see the classic powder pattern for ^{129}Xe inside a microporous solid? Three situations may be considered: (1) Each Xe is immobilized at an adsorption site, all sites deform the electron distribution of Xe atom in the same way to give rise to a unique shielding tensor. Here, the powder pattern traces out the probability of finding that particular component of the shielding tensor along the magnetic field direction (projections of components onto the magnetic field axis). Anisotropic powder patterns have been reported for Xe in a variety of clathrates and inclusion compounds where the Xe atom is truly localized, with anisotropies ranging from 15 to 170 ppm.[83] (2) Each Xe atom has sampled the entire environment inside one cage only and each cage has a specific occupancy. The Xe in each cage having a particular occupancy, say 5 Xe atoms, will have an average shielding tensor. This average shielding tensor will be different for each Xe_n and independent of overall loading. For fast intracage averaging in cages that have symmetry lower than T, T_h, T_d, O, O_h, or K_h, the average chemical shift will depend on the orientation of the cavity in the external magnetic field. A sample of containing randomly oriented crystals will then exhibit a powder pattern for each Xe_n. Because the powder pattern reflects an average shielding tensor, it will not have the span of a composite powder pattern obtained by superposition of the individual shielding tensors corresponding to frozen configurations. Examples of this are the line shapes for Xe_n in an α cage of NaA, at a temperature low enough that the effects of intercage exchange on the line shape is negligible. Since the α cages of NaA are nearly cubic, the anisotropy is small. (3) Each Xe atom has sampled many environments inside a crystallite. The Xe in each crystallite has an average shielding tensor which depends on the average number of Xe atoms per unit cell (since part of the shielding is due to Xe−Xe interactions). The powder pattern traces out the average anisotropic shielding tensor under slow exchange. The powder pattern is loading-dependent and temperature-dependent because it corresponds to an average chemical shift tensor. This is the

example in Figure 3, where the silicalite crystals are large enough that intercrystallite exchange is negligible.

We are presently unable to reproduce the powder pattern in Figure 3 by GCMC simulations because we are using only the isotropic shielding function built up from a pairwise additivity assumption. To carry out a simulation of the powder pattern, a shielding function that contains the full tensor information as a function of configurations is required in the GCMC simulations. Although the ab initio calculations of the shielding at various positions of the single rare gas atom in the zeolite cage fragment provides the full tensor, the representation of all the ab initio tensors in various positions by a single function for an arbitrary configuration has not yet been attempted. For more than one Xe atom in a cage, the tensors can be investigated by ab initio calculations of multiple rare gas atoms in the presence of a zeolite cage fragment. This has not yet been attempted.

We believe that having Xe-saturated large crystals where slow single-file diffusion takes place is giving rise to the powder pattern in silicalite. The singularities in the powder pattern δ_{11} and δ_{22} represent averages of chemical shift tensor elements, each of which has a large dispersion (range of values). From the temperature dependence of the powder pattern in Figure 6 we found an essentially constant smallest chemical shift component δ_{33}. Furthermore, the most shielded direction (smallest chemical shift relative to the free Xe atom, δ_{33}) should be along the Xe−Xe internuclear axis, coincident with the channel axis, based on previous calculations we have carried out on linear Ar_3 clusters.[21] More recent ab initio calculations give a Xe−Xe tensor with the greatest shielding (smallest chemical shift) direction along the line of centers, $(\delta_{11} - \delta_{33}) = (\sigma_{||} - \sigma_{\perp}) = 70$ ppm at 4.2 Å.[22] For loadings of 16 Xe/unit cell (saturation) the Xe atom motion is *concerted* and primarily lateral, that is, along the channel axis. At a given temperature under conditions of saturation, the Xe atoms are separated by an average distance which is small and has a small dispersion. Therefore, the shielding along the channel axis is expected to be nearly constant with temperature. Experimentally we observe that the temperature dependence of δ_{33} is nearly constant with temperature (see Figure 6) and therefore consistent with these ideas.

The width of the powder pattern in silicalite is not as large as might be expected from other Xe powder patterns (75 ppm in DD3R[86,87] or 55 ppm in ALPO-11[38]). There may be a structural reason for this. Consider the example where there are only parallel straight channels in the zeolite, with channel cross sections of the size of a Xe atom, permitting the Xe to be lined up right along the channel axis. In the fully loaded case, under slow single file diffusion, a Xe tensor is always oriented in the same way for a particular crystal orientation, and so it gives rise to a resonance which is associated with one region of a powder pattern. Silicalite has two types of channels with mutually orthogonal orientations. The chemical shift tensors in the two types of channels are probably similar when the channels are full or nearly so. Thus, the Xe tensors in the two channel types are very similar, but are oriented at 90° from each other. A Xe atom can move from one channel to a perpendicular one on the NMR time scale despite slow single-file diffusion (after all the channels are only several Angstroms apart). The Xe tensor averaging occurs between orthogonal orientations when Xe atoms move between straight and sinusoidal channels. When this happens, for a given orientation of a crystal, the resonance results from averaging $\delta_{11}^{\text{sinusoidal}}$ and $\delta_{33}^{\text{straight}}$. This leads to a dispersion in the averages that is smaller than might be expected, giving an average tensor with reduced apparent anisotropy.

C. Average ^{129}Xe Chemical Shift of Xenon Inside a Zeolite as a Function of $\langle N \rangle_{Xe}$. In our previous work in NaA we observed individual chemical shifts for specific numbers of Xe atoms in a cage. The fractions of cages containing specifically *n* Xe atoms and also the chemical shifts of these Xe_n as a function of temperature were reproduced by our GCMC simulations, as well as the adsorption isotherms. In the open zeolite networks (such as silicalite, NaY, NaX, or CaA), the Xe atoms are distributed among the cages and channels and the observed Xe chemical shift is the average that results from having visited a very large number of variously occupied cages and channels within a crystallite. Convoluted within the observed average chemical shift are the Xe chemical shifts characteristic of specific numbers of Xe atoms per cage *and* the distribution of the Xe occupancies among the cages per channels. On the basis of our previous success with the method in the Xe/NaA system where detailed tests were possible, it was our expectation that the GCMC simulations could reproduce the *trends* in the average chemical shifts as a function of loading and temperature for Xe in the open network zeolites in the present work. In the present work, no attempt was made to optimize parameters either in the potential or the shielding function to specifically obtain better simulation results for the Xe chemical shifts in faujasites. We used the same set of Lennard-Jones parameters for Xe−O and Xe-cation and the same set of partial charges as had previously been used for $Ca_xNa_{12-2x}A$, in which Si/Al = 1.0.

It is indeed encouraging that the GCMC simulations successfully reproduce the experimental data for Xe in NaY *and* NaX. It should be noted that there should be an explicit dependence of the ^{129}Xe shielding function itself upon the Si/Al ratio. This has not been taken into account in this work. Here, the Si/Al ratio has been permitted to influence the GCMC results only in the presence of Na^+ ion contributions to the Xe chemical shift and indirectly in the effect of the Si/Al ratio on the distribution of the Xe within the faujasite. Nevertheless, the average chemical shifts obtained by GCMC simulations are in good agreement with the experimental observation that the ^{129}Xe chemical shifts vary systematically with Si/Al ratio.[10] This is the first theoretical confirmation of the experimental trends found by Liu et al.,[10] in contrast with earlier observations of Ito and Fraissard.[4] The GCMC simulations produce a small but systematic dependence on the Si/Al ratio at low loadings, and the difference becomes more evident at higher $\langle N \rangle_{Xe}$, as shown in Figure 15. There is significantly more curvature in the Xe chemical shift vs $\langle N \rangle_{Xe}$ in NaY where the polarization contributions are less than in NaX. This change in the curvature has been observed also upon including polarization in the GCMC simulations of Xe in CaA.[26]

To reproduce the dependence of the Xe chemical shift on loading in silicalite depends on getting the correct distribution among the 3 different general environments within the crystallite (straight channels, sinusoidal channels, and intersections) for a given occupancy. This is sensitive to the potential function used. Different authors have found different results for the distribution of Xe in the various regions of silicalite, according to the occupancy.[42−44,46] At the same time, getting the correct average shielding also depends on using the correct Xe−O shielding function to describe the way in which the shielding of the Xe atom depends on the position within the channels. We have used the same Xe−O shielding function as we have used for Xe in NaA and $Ca_xNa_{12-2x}A$. Since the shielding function itself was derived by doing ab initio calculations of shielding using fragments of the zeolite A α cage, we did not expect to get very good agreement with the Xe chemical shifts in silicalite.

Nevertheless, using the parameter set II in V_{LJ}(Xe−O) in the GCMC simulations at room temperature and at 144 K, we find that we are able to reproduce reasonably well the experimental results not only for the adsorption isotherm but also for the average ^{129}Xe chemical shifts in the large silicalite crystals. As a test of sensitivity to potential parameters, we also tried parameter set I (faujasite and A zeolite parameters) for Xe in silicalite and verified that we could not reproduce the adsorption isotherms at 295 and 195 K for silicalite. Since the potential could not provide the proper distribution of Xe within this zeolite it also gave poor ^{129}Xe chemical shifts.

D. Temperature Dependence of the Average ^{129}Xe Chemical Shift under Fast Exchange. The temperature dependence of the average chemical shift is even more demanding to reproduce in a simulation than the chemical shift change with loading at any one temperature. This depends on being able to reproduce the change in the distribution of the Xe among the various regions of the crystallite as the temperature is varied, in accordance with the potential energy description for Xe within the zeolite. The average chemical shift reflects the two-body distribution function for Xe and the O atoms in the framework of the entire network, which gives the Xe−zeolite contributions to the shifts. The two-body distribution function for Xe−Xe, within the network, gives the Xe−Xe contributions to the chemical shifts. These two-body distributions are temperature dependent. The interaction potentials used in the simulations have to be good enough to give reasonably good descriptions of the *changes* in these two-body distribution functions with temperature. These changes are difficult to predict a priori. However, the qualitative behavior could be predicted entirely from the Xe_n in NaA model system. For the low loading samples, the temperature dependence is expected to follow that of the temperature dependence of the chemical shift of the Xe_1 peak in NaA, where a single Xe in an α cage is being observed, the chemical shift decreases with increasing temperature. This arises because the shielding function exhibits higher deshielding at shorter distances between Xe and framework atoms. The concave curved surfaces of the zeolite internal structure lead to lowest energy positions close to the walls (which correspond to greater deshielding), more or less following the contours of the inside surface. As the temperature is increased, the probability of finding the Xe at larger distances from the inner walls (which correspond to smaller deshielding) increases. Thus, the lowest loading samples are expected to have chemical shifts decreasing with increasing temperature, as long as only one kind of cavity is involved. On the other hand, in silicalite, where there are three general regions where the Xe may be found (straight channels, sinusoidal channels, and intersections), the distribution among these regions may also play a role, so the situation is not as clear as that in the faujasites and the A zeolites.

For the maximum loading samples, we might expect the same behavior with temperature as we have observed for the Xe_8 peak in NaA, the chemical shift increasing with increasing temperature. Since the crowded channels and cages permit only very short Xe−Xe distances to be averaged over, as the temperature increases while at constant occupancy, the probability of sampling inside the Xe−Xe repulsive wall increases (shorter distances between Xe atoms, corresponding to greater deshielding in the Xe−Xe shielding function). Thus, at high Xe loading, the average ^{129}Xe chemical shift in fast exchange in open network zeolites is expected to increase with increasing temperature in the same way that Xe_8 in the NaA α cage does. We do find this behavior in our GCMC simulations for Xe in NaY, NaX, and CaA. Figure 16 shows that, *for a given loading*, at low loadings the chemical shift of Xe in NaY is higher at lower temperatures; on the other hand, at high loadings the chemical shift is lower at lower temperatures. At some value of $\langle N \rangle_{Xe}$ the behavior of ^{129}Xe chemical shift with temperature *at a given loading* can be anywhere between these two cases, depending on the value of $\langle N \rangle_{Xe}$ at which the two temperature-dependent chemical shift curves cross.

For silicalite, the results of the GCMC simulations show the same behavior (see Figure 13), except that the crossing point occurs at low loading, rather than at intermediate loading. This is predicted whether we use (set I) or (set II) potential parameters for Xe−O interactions in silicalite. The GCMC simulations in Figure 13 for silicalite shows that the chemical shifts curves at 144 and 300 K cross at low loading (about 6 Xe atoms/unit cell) and diverge at higher temperatures, with the chemical shifts at higher temperature being greater (same behavior as Xe_8 in NaA).

It would be interesting to compare the general predictions stated above with the general behavior of the experimental temperature dependence of Xe chemical shifts over the full range of loadings of Xe in zeolites. However, hardly any variable temperature data on Xe chemical shifts in zeolites have been available in the literature, and even room temperature data are only available for loading levels less than about 3−4 Xe atoms/cage. The available experimental data at the low loading end are uniformly in agreement with the GCMC results that the chemical shift is greater at lower temperatures. Cheung et al. found that the Xe chemical shifts in NaY, KY, MgY, CaY, and BaY is greater at 144 K than at 293 K.[50] We reported this type of behavior also for Xe in CaA: At a given loading, the chemical shifts are higher at 240 K than at 300 K, which are higher than at 360 K.[53] However, within the errors of our data we did not observe the crossover point where the opposite behavior commences, even though we used samples with loadings up to saturation.

In the present work, we find higher chemical shifts at lower temperatures *even at maximum occupancy* in large crystals of silicalite in Figure 6. The observed temperature dependence of Xe chemical shifts at maximum loading in silicalite is in disagreement with the trend in the temperature dependence of the average Xe chemical shift obtained from GCMC simulations in Figure 13. So far, there has been no experimental observation of the behavior (higher chemical shift at higher temperature at fixed loading) that was observed and predicted for Xe_6, Xe_7, and Xe_8 in NaA[14] in any of the zeolites with open frameworks, although high loading simulations predict it for NaY, for silicalite and also for CaA.[26]

VI. Conclusions

We have observed ^{129}Xe NMR spectra of Xe from low loading up to saturation in three zeolites, silicalite, CaA, and NaX. We find that the line shapes and the apparent ^{129}Xe chemical shifts are dependent on the dynamics of the Xe in each case. Only in the large crystals of silicalite is the exchange between "inside" and "outside" Xe atoms sufficiently slow that the spectra obtained reflect the anisotropy of the average shielding tensor of the adsorbed Xe. The rate of this exchange has been measured. The adsorbed Xe is observed as a powder pattern spectrum and the temperature dependence of this powder pattern has been observed. The maximum loading we found for Xe in silicalite at room temperature, 16 Xe atoms/unit cell, agrees with the 16−17 Xe atoms/unit cell from the adsorption isotherm of Chen[45] and of Bülow et al.,[76] but does not agree

with higher estimates, up to 20 Xe atoms/unit cell, that have been derived by other workers.[41,44] The temperature dependence, the loading dependence, and the effect of Xe dynamics on the ^{129}Xe NMR line shapes in zeolites silicalite, NaX, and CaA have been determined experimentally and interpreted in terms of the behavior of various limiting cases and in terms of the various Xe reservoirs in the sample.

We have studied the adsorption isotherms and the average chemical shifts of Xe in the zeolites NaY, NaX, and silicalite as a function of loading and temperature using grand canonical Monte Carlo simulations. This interpretation of the average chemical shifts at the microscopic level using GCMC simulations may be expected to apply more generally to Xe in all open network zeolites. The agreement of the GCMC simulations with the qualitative behavior of experimental isotherms and chemical shifts with loading and temperature is good. The use of a set of parameters for the effective V_{LJ}(Xe−O) based on the PN1 potential designed by Pellenq and Nicholson for Xe in silicalite provided excellent agreement with experimental adsorption isotherms and Xe chemical shifts as a function of loading. The temperature dependence of the average chemical shift as a function of loading has been investigated by GCMC simulations in NaY, NaX, CaA, and silicalite, and was found to agree with the low-loading experimental findings where temperature-dependent studies have been carried out. Comparisons with low-temperature high-loading data are more severe tests of the potential parameters used. That the GCMC results do not agree with the experimental temperature dependence at maximum loading observed in the present work is a clear indication that we do not yet have the optimum potential parameters to describe Xe−zeolite interactions.

Acknowledgment. This work has been supported by the National Science Foundation (Grant CHE95-28066). We thank Dr. Lennox Iton for helpful discussions about zeolites.

References and Notes

(1) Fraissard, J.; Ito, T. *Zeolites* **1988**, *8*, 350.
(2) Dybowski, C.; Bansal, N.; Duncan, T. M. *Annu. Rev. Phys. Chem.* **1991**, *42*, 433.
(3) Barrie, P. J.; Klinowski, J. *Prog. Nucl. Magn. Reson. Spectrosc.* **1992**, *24*, 91.
(4) Ito, T.; Fraissard, J. *J. Chem. Phys.* **1982**, *76*, 5225.
(5) Derouane, E. G.; Nagy, J. B. *Chem. Phys. Lett.* **1987**, *137*, 341.
(6) Demarquay, J.; Fraissard, J. *Chem. Phys. Lett.* **1987**, *136*, 314.
(7) Johnson, D. W.; Griffiths, L. *Zeolites* **1987**, *7*, 484.
(8) Ripmeester, J. A.; Ratcliffe, C. I.; Tse, J. S. *J. Chem. Soc., Faraday Trans. 1* **1988**, *84*, 3731.
(9) Chen, Q.; Springuel-Huet, M. A.; Fraissard, J.; Smith, M. L.; Corbin, D. R.; Dybowski, C. *J. Phys. Chem.* **1992**, *96*, 10914.
(10) Liu, S. B.; Ma, L. J.; Lin, M. W.; Wu, J. F.; Chen, T. L. *J. Phys. Chem.* **1992**, *96*, 8120.
(11) Liu, S. B.; Fung, B. M.; Yang, T. C.; Hong, E. C.; Chang, C. T.; Shih, P. C.; Tong, F. H.; Chen, T. L. *J. Phys. Chem.* **1994**, *98*, 4393.
(12) Kim, J. G.; Kompany, T.; Ryoo, R.; Ito, T.; Fraissard, J. *Zeolites* **1994**, *14*, 427.
(13) Chmelka, B. F.; Raftery, D.; McCormick, A. V.; Menorval, L. C.; Levine, R. D.; Pines, A. *Phys. Rev. Lett.* **1991**, *66*, 580; **1991**, *67*, 931.
(14) Jameson, C. J.; Jameson, A. K.; Gerald II, R. E.; de Dios, A. C. *J. Chem. Phys.* **1992**, *96*, 1676.
(15) Ratcliffe, C. I.; Ripmeester, J. A. *J. Am. Chem. Soc.* **1995**, *117*, 1445.
(16) Jameson, C. J.; Jameson, A. K.; Gerald, R. E., II; Lim, H. M. *J. Chem. Phys.* **1995**, *103*, 8811.
(17) Jameson, C. J.; Jameson, A. K.; Baello, B. I.; Lim, H. M. *J. Chem. Phys.* **1994**, *100*, 5965.
(18) van Tassel, P. R.; Davis, H. T.; McCormick, A. V. *Mol. Phys.* **1991**, *73*, 1107.
(19) van Tassel, P. R.; Davis, H. T.; McCormick, A. V. *J. Chem. Phys.* **1994**, *98*, 8919.
(20) Li, F. Y.; Berry, R. S. *J. Phys. Chem.* **1995**, *99*, 2459.
(21) Jameson, C. J.; de Dios, A. C. *J. Chem. Phys.* **1992**, *97*, 417.
(22) de Dios, A. C.; Jameson, C. J. *J. Chem. Phys.* **1997**, *107*, 4253.
(23) Wolinski, K.; Hinton, J.; Pulay, P. *J. Am. Chem. Soc.* **1990**, *112*, 8251.
(24) Pulay, P. TEXAS: The University of Arkansas: Fayetteville, AR, 1991.
(25) Jameson, C. J.; Lim, H. M. *J. Chem. Phys.* **1995**, *103*, 3885.
(26) Jameson, C. J.; Lim, H. M.; Jameson, A. K. *Solid State Nucl. Magn. Reson.* To be published.
(27) Ripmeester, J. A.; Ratcliffe, C. I. *J. Phys. Chem.* **1990**, *94*, 7652.
(28) Samant, M. G.; de Menorval, L. C.; Dalla Betta, R. A.; Boudart, M. *J. Phys. Chem.* **1988**, *92*, 3937.
(29) Ripmeester, J. A.; Ratcliffe, C. I. In *Proceedings of the 9th International Zeolite Conference*; Montreal, 1992; von Ballmoos, R., et al., Eds.; Butterworth-Heinemann: Stoneham, MA, 1993, p 571.
(30) Jameson, C. J.; Jameson, A. K.; Lim, H. M.; Baello, B. I. *J. Chem. Phys.* **1994**, *100*, 5977.
(31) Jameson, C. J.; Lim, H. M. **1997**, *107*, 4373.
(32) Jameson, A. K.; Jameson, C. J.; Gerald, R. E., II *J. Chem. Phys.* **1994**, *101*, 1775.
(33) Larsen, R. G.; Shore, J.; Schmidt-Rohr, K.; Emsley, L.; Long, H.; Pines, A.; Janicke, M.; Chmelka, B. F. *Chem. Phys. Lett.* **1993**, *214*, 220.
(34) Moudrakovski, I. L.; Ratcliffe, C. I.; Ripmeester, J. A. In *Proceedings of the International Zeolite Symposium*; Quebec, 1995; Bonneviot, L., Kaliaguine, S., Eds.; *Studies in Surface Science and Catalysis*; Elsevier: Amsterdam, 1995; Vol. 97, p 243.
(35) Engelhardt, G.; Lohse, U.; Lippmaa, E.; Tarmak, M.; Mägi, M. *Z. Anorg. Allg. Chem.* **1981**, *482*, 49.
(36) Kuperman, A.; Nadimi, S.; Oliver, S.; Ozin, G. A.; Garces, J. M.; Olken, M. M. *Nature* **1993**, *365*, 239.
(37) Olson, D. L.; Peck, T. L.; Webb, A. G.; Magin, R. L.; Sweedler, J. V. *Science* **1995**, *270*, 1967.
(38) Ripmeester, J. A.; Ratcliffe, C. I. *J. Phys. Chem.* **1995**, *99*, 619.
(39) Jameson, C. J.; Jameson, A. K.; Cohen, S. M. *J. Chem. Phys.* **1973**, *59*, 4540.
(40) Gerald, R. E., II; Krasavin, A. O.; Botto, R. E. *J. Magn. Reson., Ser. A* **1996**, *123*, 201.
(41) Cheung, T. T. P. *J. Phys. Chem.* **1990**, *94*, 376.
(42) Pellenq, R. J−M.; Nicholson, D. *Langmuir* **1995**, *11*, 1626.
(43) Pickett, S. D.; Nowak, A. K.; Thomas, J. M.; Peterson, B. K.; Swift, J. F. P.; Cheetham, A. K.; den Ouden, C. J. J.; Smit, B.; Post, M. F. M. *J. Phys. Chem.* **1990**, *94*, 1233.
(44) El Amrani, S.; Vigne-Maeder, F.; Bigot, B. *J. Phys. Chem.* **1992**, *96*, 9417.
(45) Chen, D. Ph.D. Thesis, University of London, 1992.
(46) June, R. L.; Bell, A. T.; Theodorou, D. N. *J. Phys. Chem.* **1990**, *94*, 8232.
(47) Led, J. J.; Gesmar, H. *J. Magn. Reson.* **1982**, *49*, 444.
(48) Led, J. J.; Gesmar, H.; Abildgaard, F. *Methods Enzymol.* **1989**, *176*, 311.
(49) Jameson, A. K.; Gerald, R. E.; Jameson, C. J. To be published.
(50) Cheung, T. T. P.; Fu, C. M.; Wharry, S. *J. Phys. Chem.* **1988**, *92*, 5170.
(51) Ripmeester, J. A. *J. Am. Chem. Soc.* **1982**, *104*, 290.
(52) Gerald, R. E., II Ph.D. Thesis, University of Illinois at Chicago, 1994.
(53) Jameson, C. J.; Jameson, A. K.; Gerald II, R. E.; de Dios, A. C. *J. Chem. Phys.* **1992**, *96*, 1690.
(54) Aziz, R. A.; Slaman, M. J. *Mol. Phys.* **1986**, *57*, 825.
(55) Mezei, M. *Mol. Phys.* **1980**, *40*, 901.
(56) van Koningsveld, H.; Jansen, J. C.; van Bekkum, H. *Zeolites* **1990**, *10*, 235.
(57) van Koningsveld, H.; Jansen, J. C.; van Bekkum, H. *Zeolites* **1987**, *7*, 564.
(58) Klinowski, J.; Carpenter, T. A.; Gladden, L. F. *Zeolites* **1987**, *7*, 73.
(59) Fyfe, C. A.; Strobl, H.; Kokotailo, G. T.; Kennedy, G. J.; Barlow, G. E. *J. Am. Chem. Soc.* **1988**, *110*, 3373.
(60) Eulenberger, G. R.; Shoemaker, D. P.; Keil, J. G. *J. Phys. Chem.* **1967**, *71*, 1812.
(61) Mortier, W., J.; van den Bossche, E.; Uytterhoeven, J., B. *Zeolites* **1984**, *4*, 41.
(62) Fitch, A. N.; Jobic, H.; Renouprez, A. *J. Phys. Chem.* **1986**, *90*, 1311.
(63) Kaszkur, Z. A.; Jones, R. H.; Walter, D.; Catlow, C. R. A.; Thomas, J. M. *J. Phys. Chem.* **1993**, *97*, 426.
(64) Eddy, M. M.D. Phil. Thesis, Oxford University, 1985.
(65) Mortier, W. J. *Compilation of Extraframework Sites in Zeolites*; Butterworth Scientific Ltd.: Guildford, 1982.
(66) Smith, J. V. *Adv. Chem. Ser.* **1971**, *101*, 171.
(67) Hseu, T. Ph.D. Thesis, University of Washington, 1972 (University Microfilms No. 73-13835, Ann Arbor, Michigan).
(68) Olson, D. H. *Zeolites* **1995**, *15*, 439.
(69) Vitale, G.; Bull, L. M.; Cheetham, A. K. To be published (cited by ref 70).
(70) Auerbach, S. M.; Bull, L. M.; Henson, N. J.; Metiu, H. I.; Cheetham, A. K. *J. Phys.* **1996**, *100*, 5923.

(71) Ramdas, S.; Thomas, J. M.; Klinowski, J.; Fyfe, C. A.; Hartmann, J. S. *Nature* **1981**, *292*, 228.
(72) Klinowski, J.; Ramdas, S.; Thomas, J. M.; Fyfe, C. A.; Hartmann, J. S. *J. Chem. Soc., Faraday Trans. 2* **1982**, *78*, 1025.
(73) Melchior, M. T.; Vaughan, D. E. W.; Pictroski, C. F. *J. Phys. Chem*. **1995**, *99*, 6128.
(74) Pellenq, R. J−M.; Nicholson, D. *J. Phys. Chem*. **1994**, *98*, 13339.
(75) Tsiao, C.; Corbin, D. R.; Durante, V.; Walker, D.; Dybowski, C. *J. Phys. Chem*. **1990**, *94*, 4195.
(76) Bülow, M.; Hartel, U.; Müller, U.; Unger, K. K. *Ber. Bunsen-Ges. Phys. Chem*. **1990**, *94*, 74.
(77) Fomkin, A. A.; Serpinski, V. V.; Bering, B. P. *Bull. Acad. Sci. USSR, Div. Chem. Sci*. **1975**, *24*, 1147.
(78) Liu, S. B. Private communications.
(79) Boddenberg, B.; Hartman, M. *Chem. Phys. Lett*. **1993**, *203*, 243.
(80) Gupta, V.; Davis, H. T.; McCormick, A. V. *J. Phys. Chem*. **1996**, *100*, 9824.
(81) Chitra, R.; Yashonath, S. *Chem. Phys. Lett*. **1995**, *234*, 16.
(82) Mosell, T.; Schrimpf, G.; Hahn, C.; Brickmann, J. *J. Phys. Chem*. **1996**, *100*, 4571.
(83) Davidson, D. W.; Ripmeester, J. A. In *Inclusion Compounds*; Artwood, J. L., Davies, J. E. D., MacNicol, D. D., Eds.; Academic Press: New York, 1984.
(84) Buckingham, A. D.; Malm, S. M. *Mol. Phys*. **1971**, *22*, 1127.
(85) Jameson, A. K.; Jameson, C. J.; de Dios, A. C.; Oldfield, E.; Gerald, R. E., II; Turner, G. L. *Solid State Nucl. Magn. Reson.* **1995**, *4*, 1.
(86) Ripmeester, J. A.; Ratcliffe, C. I. In *Proceedings of the 8th International Zeolite Conference*; Amsterdam, 1989; Jacobs, P. A., van Santen, R. A., Eds.; *Studies in Surface Science and Catalysis*; Elsevier: Amsterdam, 1989; Vol. 49B.
(87) Ripmeester, J. A.; Ratcliffe, C. I. *Mater. Res. Soc. Symp. Proc*. **1991**, *233*, 281.
(88) Hahn, K.; Kärger, J. *J. Phys. Chem*. **1996**, *100*, 316.
(89) Heink, W.; Kärger, J.; Pfeiffer, H.; Stallmach, F. *J. Am. Chem. Soc*. **1990**, *112*, 2175.
(90) Chen, Q. J.; Fraissard, J. *J. Phys. Chem*. **1992**, *96*, 1809.
(91) Tway, C.; Apple, T. *J. Catalysis* **1992**, *133*, 42.
(92) Ripmeester, J. A.; Ratcliffe, C. I. *Anal. Chim. Acta* **1993**, *283*, 1103.
Received March 20, 1997. In Final Form July 7, 1997.